INSTITUTO POLITÉCNICO NACIONAL

Centro Interdisciplinario de Investigación

para el Desarrollo Integral Regional Unidad Oaxaca

Doctorado en ciencias en conservación

y aprovechamiento de recursos naturales

(Patrones y procesos para la biodiversidad del neotrópico)

Estudio de señales ultrasónicas de materiales basados en cemento durante procesos de hidratación, carbonatación y penetración de cloruros

Tesis que para obtener el grado académico de:

Doctor en ciencias

Presenta:

M. en C. Mario Fernando Cosmes López

Directores de tesis:

Dr. Francisco Castellanos León

Dr. Prisciliano Felipe de Jesús Cano Barrita

Índice

Introducción general

El concrete es una pieza clave en la industria de la construcción en todo el mundo, como carreteras, presas, puentes, edificios, entre otros. Dichas estructuras están continuamente sujetas a efectos que degradan su integridad estructural provocando un riesgo de seguridad, por lo tanto, se deben desarrollar alternativas para una evaluación efectiva de su calidad sin la necesidad de dañar las estructuras estudiadas [1].

En este sentido, el uso de pruebas no destructivas constituye una interesante estrategia para el monitoreo y evaluación del estado de las estructuras de concreto sin dañar su apariencia o rendimiento [2]. Las pruebas no destructivas con ultrasonido se basan en la propagación de ondas a través del elemento analizado y han sido ampliamente aplicadas en estructuras de concreto [3,4]. La velocidad de propagación de las ondas ultrasónicas depende de distintas características del material como: densidad, módulo de elasticidad (E) y coeficiente de Poisson, (μ); sus principales aplicaciones son la detección de daños y evaluación de condiciones iniciales del concreto [5].

En general la aplicación de los análisis no destructivos por ultrasonido se ha hecho usando dos métodos convencionales, la transmisión directa y el pulso eco [6]. En el método de transmisión se realiza la medición en lados opuestos de la estructura, para conocer el tiempo de recorrido que junto con la distancia recorrida nos permite conocer la Velocidad de Pulso Ultrasónico (UPV). El pulso eco, mide la reflexión por medio del mismo u otros transductores que actúan como receptores del pulso ultrasónico. Las pruebas anteriores se han estandarizado por medio de

procedimientos, instrumentaciones y análisis de datos para distintos tipos de ondas aplicadas a estructuras de concreto [7].

Cualquier variación en la velocidad de propagación de las ondas ultrasónicas indican vacíos, no uniformidad del material o daños [8,9]. Como señalan varios autores [10,11,12], las ondas ultrasónicas pueden verse afectados por varios factores, como la condición superficial, la humedad, la presencia de refuerzos y principalmente la composición del concreto. Tales factores provocan variaciones no solo en la velocidad de propagación de las ondas ultrasónicas, sino también en la señal en el tiempo, lo que dificulta el análisis de resultados [13]. Sin embargo, este hecho abre una ventana de oportunidad para poder conocer otras propiedades además del VPU, que permitan la evaluación de distintos fenómenos de una manera completamente no destructiva.

Debido a que la mayor cantidad de reacciones que suceden dentro del concreto se llevan a cabo en la pasta de cemento, el siguiente trabajo se centra en el análisis del comportamiento de la pasta de cemento en distintas condiciones, por medio de ondas longitudinales y transversales, con un intervalo de frecuencia de 50 kHz a 2250 kHz. Este trabajo se encuentra dividido en tres partes:

La primera parte, presenta el estudio de especiemos de concreto con el objetivo de identificar frecuencias especificas relacionadas con agregados y pasta de cemento durante la hidratación del concreto, por medio del análisis de transformada de Fourier de la respuesta ultrasónica de especímenes de concreto con diferentes frecuencias de excitación. Con lo que fue posible identificar el comportamiento de la pasta de cemento y agregados en el dominio de la frecuencia.

En la segunda parte, se estudió la respuesta ultrasónica en pastas de cemento con tres relaciones agua cemento (a/c = 0.60, 0.50 y 0.40). Los especímenes fueron expuestos a la carbonatación acelerada en una cámara ambiental a 30 ℃, 65% de humedad relativa, y 4% CO_2 (v / v). Los resultados muestran que es posible evaluar el grado de carbonatación de los especímenes de pasta de cemento por medio del análisis en el dominio de frecuencia en función del tiempo de exposición, de los cambios relacionados a la carbonatación, independientemente de la relación agua / cemento.

La tercera parte presenta, presenta el estudio de dieciocho especímenes de pasta de cemento con una relación a / c = 0.55, con 100% de cemento Portland ordinario, sustitución del 20% y 40% de cemento por cenizas volantes de clase F y sustitución al 10% por humo de sílice. Los especímenes fueron secados en horno y saturados a 4,08 bar con soluciones de NaCl de 16,5% (2,8 M), 33% (5,6 M) y una con agua desionizada, como control. Los resultados muestran que, aplicando la metodología utilizada en las secciones anteriores y tomando como base los resultados del control, es posible distinguir entre las dos concentraciones de NaCl independientemente de las adiciones minerales y entre las pastas de cemento con adiciones minerales dependiendo de su capacidad de ligado.

Referencias

[1]. Mehta, P. K. (1986). Concrete. Structure, properties and materials.

[2]. Hoła, J., & Schabowicz, K. (2010). State-of-the-art non-destructive methods for diagnostic testing of building structures–anticipated development trends. Archives of Civil and Mechanical Engineering, 10(3), 5-18.

[3]. Philippidis, T. P., & Aggelis, D. G. (2003). An acousto-ultrasonic approach for the determination of water-to-cement ratio in concrete. Cement and Concrete Research, 33(4), 525-538.

[4]. Lai, W. L., Wang, Y. H., Kou, S. C., & Poon, C. S. (2013). Dispersion of ultrasonic guided surface wave by honeycomb in early-aged concrete. NDT & E International, 57, 7-16.

[5]. Panesar, D. K., & Chidiac, S. E. (2007). Ultrasonic pulse velocity for determining the early age properties of dry-cast concrete containing ground granulated blast-furnace slag. Canadian Journal of Civil Engineering, 34(5), 682-685.

[6]. Malhotra, V. M., & Carino, N. J. (2003). Handbook on Nondestructive Testing of Concrete Second Edition. CRC press.

[7]. Davis, A. G., Ansari, F., Gaynor, R. D., Lozen, K. M., Rowe, T. J., Caratin, H., ... & Hertlein, B. H. (1998). Nondestructive test methods for evaluation of concrete in structures. American Concrete Institute, ACI, 228.

[8]. Whitehurst, E. A. (1986). Evaluation of concrete properties from sonic tests. ACI Monograph, 2, 73.

[9]. Carino, N. J. (1997). Nondestructive test methods. Concrete construction engineering handbook, 1.

[10]. Popovics, J. S. (2003). NDE techniques for concrete and masonry structures. Progress in Structural Engineering and Materials, 5(2), 49-59.

[11]. Schabowicz, K. (2014). Ultrasonic tomography–the latest nondestructive technique for testing concrete members–description, test methodology, application example. archives of civil and mechanical engineering, 14(2), 295-303.

[12]. Schabowicz, K., & Suvorov, V. (2014). Non-destructive testing and constructing profiles of back walls by means of ultrasonic tomography. Russian J. Non-destructive Testing, 50(2), 109-119.

[13]. Abo-Qudais, S. A. (2005). Effect of concrete mixing parameters on propagation of ultrasonic waves. Construction and building materials, 19(4), 257-263.

1   *Capítulo I*

2   Ultrasound frequency analysis for identification of aggregates and cement

3   paste in concrete

4   Mario F. Cosmes-López[1], Francisco Castellanos[2*], Prisciliano F. de J.

5   Cano-Barrita[2]

6   [1] *PhD student at Instituto Politecnico Nacional, CIIDIR Unidad Oaxaca, Hornos No.*

7   *1003, Santa Cruz Xoxocotlán, Oaxaca, Mexico, C.P. 71230.*

8   [2] *Researcher at Instituto Politecnico Nacional, CIIDIR Unidad Oaxaca, Hornos No.*

9   *1003, Santa Cruz Xoxocotlán, Oaxaca, Mexico, C.P. 71230.*

10   Phone: + 52 951 5170610, Emails: mcosmesl1200@alumno.ipn.mx,

11   fcastellanos@ipn.mx and pcano@ipn.mx

12   *Corresponding author

13

14   **Abstract**

15   The aim of the present study was to identify specific frequencies related to aggregates

16   and cement paste during concrete hydration, by performing a Fourier analysis of the

17   ultrasonic response of concrete specimens to different excitation frequencies. This

18   identification will reduce the high influence of aggregates in the ultrasound signal

19   analysis, enabling a better assessment of changes occurring in the cement paste. Thirty-

20   five cylindrical specimens with a diameter of 100 mm and a length of 200 mm were cast

21   with a water to cement ratio = 0.60. Thirty specimens were destructively tested at 1, 3,

22   5, 7, 14 and 28 days for their compressive strength. The remaining five specimens were

23   non-destrudtive tested at 1, 3, 5, 7, 14, 28 and 56 days using longitudinal and

24   transversal ultrasonic wave transducers with frequencies from 50 kHz to 500 kHz.

25   Analysis of the evolution in frequency observed in the specimens identified variations

26   related to progressive hydration of the cement paste, in contrast with the invariant

27   behavior of the inert aggregates. Results show that it is possible to distinguish the

28   behavior of cement paste and aggregates in the frequency domain. As a consequence, it

29   should be possible in future research to evaluate more efficiently different phenomena

30   that affect only the cement paste.

31   **Keywords**

33

1. Introduction

Non-destructive techniques are used to evaluate the quality and performance of concrete structures without causing any structural damage [1, 2]. The Ultrasonic Pulse Velocity (UPV) is one of the most used non-destructive techniques for measuring mechanical properties of concrete during hydration and evaluating damage in concrete structures [3-6]. Previous studies have found an exponential relationship between the compressive strength of concrete and the UPV, which has shown to be barely sensitive to small variations in strength at late ages [7-8]. Concrete is basically composed of a mixture of cement, water, fine and coarse aggregates that produce a heterogeneous material. The heterogeneities produced by the coarse aggregates strongly influence the propagation of ultrasonic waves, depending on the frequency studied [9]. Therefore, the analysis of changes in an ultrasound wave propagated across a concrete specimen at selected frequencies, may be used to extract information on processes occurring mainly in the cement paste, for example during hydration or during chemical reactions in the cement paste with aggressive species (e.g. chlorides and CO_2).

When a wave propagates, its phase and amplitude are modified depending on the transmission medium. The propagation of ultrasound waves is affected by the heterogeneities of concrete in different ways. The influence depends on the wavelength and the size of the concrete components [10]. In previous studies, this behavior was used to characterize entrained air voids in cement paste [11]. Other studies have employed the propagation velocity of the wave attenuation to estimate cracking [12-14], voids, the setting process [15, 16] and the compressive strength of concrete. Taking advantage of these properties, several experimental studies using through-transmission ultrasonic measurements of longitudinal or transversal waves have been carried out on

58 concrete to determine the setting time of concrete [4,17]. It has also been found that the

59 attenuation of the ultrasound signal is different for cement paste, mortar and concrete in

60 a frequency range of 50 - 1000 kHz [18-19]. Additionally, the setting process of cement

61 pastes has been analyzed by the response of ultrasonic waves using the frequency

62 spectrum of the Fast Fourier Transform [20].

63 Based on the aforementioned, it is assumed that, depending on the frequency band used,

64 the response of concrete materials to ultrasonic waves contains more information than is

65 reported. Therefore, this study focuses on developing a method for the identification of

66 frequency bands associated with aggregate and cement paste during the hydration

67 process of concrete. This identification would enhance the study of process which occur

68 only in the cement paste such as hydration, chloride penetration and binding as well as

69 carbonation produced by the chemical reaction between the CO_2 and $Ca(OH)_2$ dissolved

70 in the pore fluid.

71 **2. Experimental procedure**

72 **2.1. Materials**

73 Mexican ordinary Portland cement class 30RS (ASTM C150 Type I or EN 197-I, with

74 chemical composition shown in Table 1) was used. The coarse aggregate was limestone

75 with a maximum size of 13 mm. The fine aggregate was river sand with a fineness

76 module of 2.67. Thirty-five cylindrical specimens measuring 100 mm in diameter and

77 200 mm in height were cast with a w/c ratio of 0.60. After 1 day, the specimens were

78 stripped and moist-cured in a saturated lime solution at 23 ± 2 °C for 56 days, according

79 to the standard ASTM C31 [21]. Moist curing with saturated lime solution avoids

80 leaching of the calcium hydroxide from the cement paste, which otherwise would

81 increase the porosity and reduce the density and elastic modulus of the cement paste.

82 **2.2. Methods**

83 **2.2.1. Compressive strength**

84 Thirty specimens were tested at 1, 3, 5, 7, 14, and 28 days to measure their compressive

85 strength using a 120 ton compression machine.

86 **2.2.2. Ultrasonic measurements**

87 Five specimens were tested at 1, 3, 5, 7, 14, 28 and 56 days. The ends of the specimens

88 were cut with a concrete saw in order to obtain a smooth surface. A record was

89 maintained of their responses in through-transmission to longitudinal and transversal

90 ultrasonic waves, generated by eight pairs of transducers with frequencies ranging from

91 50 kHz to 500 kHz. The position of the transducers and their applied pressure were kept

92 constant during the experiment. Petroleum jelly was used as coupling agent to improve

93 wave transmission. The excitation signal was generated by a 5058PR pulser/receiver

94 with a voltage of 200 V and damping of 40 dB. The UPV was also obtained for the

95 thirty specimens before compressive strength testing.

96 # 3. Wave analysis

97 ## 3.1. Signal processing

98 The aim of the proposed method for analyzing the ultrasound signals is to identify

99 frequency bands over time associated with aggregates and cement paste in hydraulic

100 concrete. One of the features of concrete is that the properties of the hydrating cement

101   paste vary over time as opposed to those of aggregates which are invariant over time.

102   The Fast Fourier Transform (FFT) has been recognized as a standard signal processing

103   technique for analyzing ultrasound signals [22]. The first step in the proposed analysis

104   is to calculate the time-discrete Fourier Transform (TDFT) of the ultrasound signal

105    $f(n\Delta t)$, according to Eq. (1).

106    $\quad$ $F(k\Delta\omega) = \frac{1}{2\pi}\sum_n f(n\Delta t)e^{-i(2\pi kn/N)}\Delta t$ $\hfill$ (1)

107   where T is the duration of the ultrasound signal, discretized at a sampling rate $\Delta t{=}T{/}N$,

108   and $k\Delta w$ are the resulting discrete frequencies.

109   A window of $F(k\Delta\omega)$ is subsequently selected from the frequency response function of

110   the transducers with an intensity greater or equal to 6 dB, as specified by the ultrasound

111   transducer manufacturer.

112    $\quad$ $G(k\Delta\omega) = \begin{cases} F(k\Delta\omega), & k_1 \leq k \leq k_2 \\ 0, & elsewhere \end{cases}$ $\hfill$ (2)

113   The evolution in time of the seven spectra obtained (1, 3, 5, 7, 14, 28 and 56 days) from

114   ultrasound measurements$G_i(k\Delta\omega)$ $G_i(k\Delta\omega)$, where $1 \leq i \leq 7$, was analyzed for the

115   identification of frequency bands associated with aggregates or cement pastes. This

116   analysis consists of the correlation of variations along time of every frequency

117   amplitude $|G_i(k\Delta\omega)|$, with a function that describes an assumed behavior of aggregates

118   or cement pastes. For the identification of frequencies k_a associated with aggregates, a

119   correlation with a constant function different from zero was performed. In the case of

120   frequencies k_p related to cement pastes, they were correlated with the evolution in time

121   of the compressive strength that indicates the progress of cement hydration, Fig. 1. The

122   compressive strength was determined according to the standard ASTM C39 / C39M –

123   16 [23]. The load was applied at a rate of 0.25 ± 0.05 MPa/s (35 ± 7 psi/s).

124   Evolution of the compressive strength of concrete is closely related to density (ρ)

125   changes in the hydrating cement paste, influencing the propagation of the ultrasonic

126   waves [2]. Constant density of limestone aggregate ($\rho = 2.60$ kg/m^3), of sand ($\rho = 2.57$

127   kg/m^3) and of saturated concrete were obtained, Fig. 1. A strong correlation coefficient

128   (R=0.98) states the evident similarity between density and compressive strength

129   evolution in time. Similarly, a strong correlation (R=0.984) was found between the

130   compressive strength of concrete (f'c) and UPV.

131   Once the assumed behavior for cement paste was identified, a threshold was defined as

132   the mean value of the correlations obtained, with a precision of 0.001, for the

133   identification of cement paste or aggregates, assuming a normal distribution for those

134   values. The frequencies with correlations stronger than the threshold were assumed to

135   be related to the corresponding behavior of cement paste or aggregates. As the

136   thresholds for both identifications were independently established, there were atypical

137   frequencies identified with both behaviors that were excluded from the analysis. Finally,

138   the correlations between the energy (E_i) and the functions that describe the assumed

139   behavior were calculated

140    $$E_i = \sum_{\forall j} |G_i(k_j \Delta\omega)|^2 \tag{3}$$

141   where j denotes the frequencies associated with paste or aggregates, respectively. The

142   time evolution of the calculated energy must be consistent with the corresponding

143   assumed behavior. The wave attenuation and wavelength analysis are two alternative

144   validations of the proposed method for identifying cement paste and aggregates,

145   presented in the following sections.

146   **3.2. Wave attenuation analysis**

147   The different components in concrete induce a high attenuation mainly correlated with

148   the size of aggregates. This attenuation α is defined as [24]

149    $$\alpha = -\frac{20}{x} log\left(\frac{A_x}{A_0}\right) \tag{4}$$

150   where A_0 is the initial amplitude of the wave and A_x is the amplitude after the wave has

151   traveled across the length x.

152   By using Eq. (4), different attenuation responses were related to cement paste, mortar

153   and concrete [19]. These different behaviors can be utilized to distinguish between

154   concrete and cement paste depending on the frequency used. The attenuation can be

155   correlated with the scattering of ultrasonic waves through the material, and in the case

156   of concrete, this scattering has been linked to the presence of aggregates [19].

157   Philippidis and Aggelis [19] found that the attenuation in cement paste specimens is

158   higher in low frequencies than in high frequencies relative to the attenuation obtained in

159   concrete specimens. Other studies support these findings [18, 25]. If the identified

160   frequency bands are representative of the hardening process of the cement paste or the

161   time invariant behavior of aggregates, then a comparison between the total energy of the

162   signal and the energy of cement paste and aggregates must present a similar behavior of

163   attenuation described in previous works [18, 19, 25]. This comparison was made

164   possible by modifying Eq. (4) as follows.

165     $\alpha_{CP} = -\frac{20}{185} log \left(\frac{E_{CP}}{E_o}\right)$ (5)

166     $\alpha_A = -\frac{20}{185} log \left(\frac{E_A}{E_o}\right)$ (6)

167   where α_{CP} and α_A are the cement paste and aggregates attenuation, respectively. E_{CP}

168   and E_A is the energy of the cement paste and aggregate frequency bands, respectively.

169   E_o is the total energy of the signal and the mean length of the specimens were 185 mm.

170   **3.3. Wavelength analysis**

171   The wavelength λ depends on wave velocity (*UPV*) and transducer frequency (*Ω)*

172   according to

173     $\lambda = \frac{UPV}{\Omega}$ (7)

174   The size of discontinuities in concrete detected by ultrasound signals depends on its

175   wavelength [26]. The sensitivity for detecting a discontinuity of a given size increases

176   with higher frequencies as the wavelength decreases, assuming constant *UPV*. Concrete

177   contains approximately 65 – 70 % of aggregates and 30 – 35% of cement paste by

178   volume. This generates a thin and continuous layer of cement paste covering and filling

179   the empty spaces among aggregates. Therefore, the wavelengths produced by low

180   frequency transducers are more sensitive for detecting aggregates than cement paste, in

181   contrast to high frequency transducers, which preferentially detect cement paste.

182   For the case of concrete, the ratio of transducer diameter (D) to the wavelength of the

183   transmitted wave (λ) can be used to determine the radiation pattern (β) of the stress

184   pulse in concrete, according to [27],

14

185 $$\beta = \frac{D}{\lambda} \tag{8}$$

186 Most of the energy transmitted into the test specimen is contained within a cone-shaped

187 region that has its base at the transducer surface and its highest amplitude in the normal

188 direction of the transducer surface. The radiation pattern for each transducer, as well as

189 its diameter are shown in Table 2. The radiation pattern mainly influences the wave

190 reflection from the boundaries of the specimen. In our experiments, as the β index

191 increases, it is expected that the wave reflected from boundaries of the specimen would

192 decrease, as well as its influence on the received signal. This influence diminishes even

193 more for higher frequencies due to the high attenuation of concrete [19]. However,

194 further studies on the effect of radiation pattern on our experiments, under similar

195 conditions, are necessary.

196 **4. Results and discussion**

197 **4.1. Frequency-domain identification of aggregates and cement paste**

198 Some typical results on the identification of frequencies related to cement paste and

199 aggregates are shown in Figs. 2 to 5. The rest of the figures are found in appendix A.

200 The frequencies associated with cement paste or aggregates are those with amplitudes

201 higher than zero in the corresponding testing age-frequency plots. The close proximity

202 of characteristic frequency bands of cement paste and aggregates can be explained by

203 similar values of the modulus of elasticity of limestone aggregates (10.8 GPa) [28] and

204 cement paste with a w/c = 0.60 (13.38 GPa) [29]. This property has a significant

205 influence on the ultrasonic response of any material, especially for those subjected to

206 longitudinal waves. The response obtained from transducers with the same frequency

207 but with different types of wave, show that the response of a transversal wave has a

208 better definition of the frequency bands related to cement paste and aggregates, as can

209 be seen by comparing Figs. 2 to 5.

210 *4.2.* **Estimation of energy evolution over time of selected frequency bands for**

211 **aggregates and cement paste**

212 It is expected that the energy associated with aggregates remains constant in time, while

213 the energy related to cement paste is assumed to increase, according to the changes in its

214 compressive strength or density. Fig. 6 (transversal wave transducers) and Fig. 7

215 (longitudinal wave transducers) present the evolution in time of energies produced by

216 different frequency transducers and types of waves. The energies are calculated for the

217 identified frequency bands and are related to the cement paste and to the aggregates. In

218 Fig. 6a, it is shown that for the 50 kHz transducers, the energy associated with

219 aggregates is higher than that associated with cement paste, in contrast to the other

220 frequencies shown in the same figure. There it is shown that, at times no later than 14

221 days after casting, the energy of cement paste reaches higher values than those values

222 corresponding to aggregates. This behavior may be attributed to the higher value of the

223 wavelength (53 mm at early stages) of the 50 kHz transversal transducer in comparison

224 with the rest of the transducers. As a consequence, the ultrasound waves collect

225 information from larger particles such as aggregates (maximum aggregate size of 13

226 mm) rather than cement paste in the specimen. This phenomenon is accentuated because

227 concrete is constituted by approximately 65-70% aggregates and 35-30% cement paste

228 by volume, and as wavelength increases with cement paste hardening.

229   Fig. 7 shows the results for the longitudinal wave transducers. It is observed that the

230   energy associated with cement paste is always higher than the energy of the aggregates

231   after three days of age. This behavior can be attributed to the higher sensitivity of

232   longitudinal waves to changes in density during concrete hardening, in comparison with

233   transversal transducers. This is due to the fact that longitudinal waves which propagate

234   in fluids and solids, have a greater interaction with the cement paste hardening in time,

235   which is reflected in the corresponding energy increase.

236   *4.3.* **Wave attenuation**

237   The analysis of the attenuation was performed to increase the certainty that the energy

238   bands are in fact related to the hardening process of cement paste and to aggregates.

239   The attenuation obtained from the energy associated with the frequency bands which

240   were identified as cement paste or aggregates (Fig. 8a) is also consistent with results

241   obtained by previous research [18, 19, 25]. It was found a direct correlation between the

242   addition of aggregates and a higher attenuation of concrete in high frequencies relative

243   to that of cement paste, as opposed to the higher attenuation associated with cement

244   paste in low frequencies. For the longitudinal wave transducers, the resulting

245   attenuation is similar to that obtained for transversal waves in the range of studied

246   frequencies, where the aggregates attenuation is always higher relative to the cement

247   paste attenuation (Fig. 8b).

248   The attenuation obtained for transversal wave transducers is shown in Fig. 8a, which

249   yielded results as expected [18, 19, 25] with a higher attenuation of cement paste energy

250   than aggregates energy in low frequencies; however, as the frequencies increase, they

251   have a similar behavior until the attenuation of aggregates energy is higher in

252 comparison with cement paste energy at frequencies corresponding to 500 kHz

253 transversal wave transducer.

254 In the case of longitudinal wave transducers (Fig. 8b), tested only with high frequencies,

255 an evident attenuation difference between cement paste and aggregates can be

256 appreciated, showing the higher attenuation of the aggregates energy bands in

257 comparison with the cement paste energy bands in every transducer employed.

258 The average attenuation associated with the hardening of the cement paste for the

259 longitudinal wave transducers is lower than that obtained for the transversal wave

260 transducers. As the energy of frequency bands was used for the estimation of

261 attenuation, due to the propagation properties of the wave, this behavior highlights the

262 higher energy of the cement paste frequency bands obtained with the longitudinal wave

263 transducer. In the case of the aggregates, the average attenuation obtained in 100, 250

264 and 500 kHz is similar for both wave type transducers.

265 *4.4.* **Wavelength analysis**

266 Wavelength depends on the frequency and the velocity of the wave Eq. (7). In turn,

267 wave velocity propagation is a function of the properties of the materials such as density

268 (ρ), elastic modulus for longitudinal and shear modulus for transversal waves related to

269 the concrete hardening [30]. These changes in the material are described by different

270 wavelengths which influence the ability to differentiate between cement paste hardening

271 and aggregates [31, 32]. The wavelengths obtained for this experiment are shown in

272 Table 2.

273   Variations in wavelength for a given frequency, Table 2, are caused by the evolution of

274   the hardening cement paste in concrete. These wavelength values are consistent with the

275   energy behavior presented in Fig. 6 and Fig. 7.

276   In the case of the 50 kHz transversal wave transducers, produced a higher energy

277   associated with aggregates, than that produced with cement paste (Fig. 6a). This is

278   because of the wavelengths associated with this frequency (56.9 ± 0.22 mm) which have

279   a higher interaction with aggregates (maximum size of 13 mm) than with cement paste,

280   in addition to a higher volume percentage of aggregates in concrete (70%). As a

281   consequence, the attenuation related to the cement paste for this low frequency

282   transducer is high Fig. 8a.

283   In contrast, the 500 kHz transversal wave transducers, with wavelengths of 3.6 ± 0.02

284   mm, produce a higher energy associated with cement paste than with aggregates (Fig.

285   6e) resulting in an opposite attenuation behavior. The rest of the frequencies (Figs. 6b -

286   6d) present a transitional behavior between these two extremes. The resulting

287   attenuation behaviors (Fig. 8a) are consistent with previous works [18, 19, 25].

288   Additionally, the sensitivity of transversal wave transducers can be considered to remain

289   constant through evaluation days as shown in the corresponding standard deviation

290   (Table 2).

291   Regarding the longitudinal waves, the increase in wavelength in comparison with

292   transversal waves, is directly proportional to their higher velocity [33] assuming a

293   constant frequency Eq. (7). This increase is more remarkable at late ages in 250 kHz

294   and 500 kHz frequency transducers and proportional to their standard deviations (Table

295   2). The constant sensitivity of transversal wave transducer allows a better evaluation of

296 the hardening process of the cement paste at late ages in contrast to the sensitivity of

297 longitudinal wave which decreases in time proportional to their standard deviations,

298 especially at high frequencies such as 500 kHz.

299 The wavelength of the longitudinal wave transducers employed (100 – 500 kHz) is

300 similar to those wavelengths corresponding to transitional attenuation behavior obtained

301 for 100 – 250 kHz transversal wave transducers (Table 2 and Fig. 8a). Therefore, the

302 attenuation behavior of longitudinal waves is inconsistent with previous works [18, 19,

303 25], however if higher and lower frequencies are employed, the attenuation behavior is

304 expected to be consistent.

305 **5. Conclusions**

306 Analysis of the results in the present paper allows for the following conclusions:

307 (1) The proposed signal analysis procedure allows for the identification of

308   frequency bands related to cement paste and aggregates, whose assumed

309   behavior in time is depicted by the evolution of compressive strength and a

310   constant function, respectively. The attenuation analysis of frequency bands

311   associated with cement paste and aggregates is consistent with previous

312   research.

313 (2) In this study, due to their high correlation, UPV might be used to describe the

314   behavior associated with cement paste instead of the actual compressive

315   strength.

316 (3) Transversal wave transducers (especially at 250 kHz) allow for a better

317   definition of the frequency bands associated with the cement paste and

318   aggregates. In addition, there is a higher correlation with attenuation in

319   comparison with the longitudinal wave transducers.

320 (4) During the hydration of concrete, the smaller variations in the wavelength of

321   transversal waves provide a higher sensitivity for detecting frequency bands

322   associated with cement paste and aggregates in comparison with those

323   obtained for longitudinal waves.

324 **Future work**

325 Research is under way aimed to improve non-destructive assessment of compressive

326 strength by applying the method outlined in this paper. It will also be applied for

327 detecting chemical reactions that only occur in the cement paste caused by aggressive

328 species such as chloride ions and carbon dioxide.

329 **Acknowledgements**

336 **References**

337 [1] J. H. Bungey, The validity of ultrasonic pulse velocity testing of in-place

338   concrete for strength, NDT&E Int. 13 (1980), 296-300.

339 [2] S. Popovics, J.L. Rose, J.S. Popovics, The behaviour of ultrasonic pulse in

340   concrete, Cem. Concr. Res. 20 (1990), 259–270.

341 [3] J. Hoła, K. Schabowicz, State-of-the-art non-destructive methods for

342   diagnostic testing of building structures – anticipated development trends,

343   Archives of Civ. Mech. Eng. 10 (2010), 5–18.

344 [4] E.A. Whitehurst, Evaluation of concrete properties from sonic tests, first

345   ed., Purdue Engineering Experiment Station, Michigan, 2011.

346 [5] G. Trtnik, M. Gams, Recent advances of ultrasonic testing of cement based

347   materials at early ages, Ultrasonics 54 (2014), 66-75.

348 [6] V.R. Sturrup, F.J. Vecchio, H. Caratin, Pulse Velocity as a Measure of

349   Concrete Compressive Strength, Am. Concr. Inst. 82 (1984), 201-228.

350 [7] A. Galan, Combined ultrasound methods of concrete testing, NDT&E Int.

351   30 (1997), 262-262.

352 [8] M.P. Ismail, K.M. Yusof, A.N. Ibrahim, A combined ultrasonic method on

353   the estimation of compressive concrete strength, INSIGHT 38 (1996), 781–

354   785.

355 [9] M.F. Kaplan, The effects of age and water to cement ratio upon the relation

356   between ultrasonic pulse velocity and compressive strength of concrete,

357   Mag. Concr. Res. 11 (1959), 85-92.

358 [10] V. Métaisa, M. Chekroun, L. Le Marrec, A. Le Duffb, G. Plantierb, O.

359   Abrahama, Influence of multiple scattering in heterogeneous concrete on

360   results of the surface wave inverse problem, NDT&E Int. 79 (2016) 53–62.

361   [11] W. Punuraia, J. Jarzynskib, J. Qub, K. E. Kurtisa, L. J. Jacobs,

362   Characterization of entrained air voids in cement paste with scattered

363   ultrasound, NDT&E Int. 39 (2006) 514–524.

364   [12] J.H. Kim, H.G. Kwak, J. Min, Characterization of the crack depth in

365   concrete using self-compensating frequency response function, NDT&E Int.

366   43 (2010), 375–384.

367   [13] H.J. Yim, H.G. Kwak, J.H. Kim, Wave attenuation measurement technique

368   for nondestructive evaluation of concrete, NDT&E Int. 27 (2012), 81–94.

369   [14] S.F. Selleck, E.N. Landis, M.L. Peterson, Shah S.P., Achenbach J.D.,

370   Ultrasonic investigation of concrete with distributed damage, Am. Concr.

371   Inst. 95 (1998), 27–36.

372   [15] P.B. Nagy, Fatigue damage assessment by nonlinear ultrasonic materials

373   characterization, Ultrasonics 36 (1998), 375–381.

374   [16] I. Gabrijel, D. Mikulić, B. Milovanović, Application of ultrasonic

375   measurements for determination of setting and hardening in cement paste, J.

376   Civ. Eng. Architecture 53 (2011), 278–283.

377   [17] S. Sharmaa, A. Mukherjee, Ultrasonic guided waves for monitoring the

378   setting process of concretes with varying workabilities, Constr. Build.

379   Mater. 72 (2014), 358-366.

380   [18] E.N. Landis, S.P. Shah, Frequency-dependent stress wave attenuation in

381   cement-based materials, J. Eng. Mech. 121 (1995), 737–743.

382   [19] T.P. Philippidis, D.G. Aggelis, Experimental study of wave dispersion and

383   attenuation in concrete, Ultrasonics 43 (2005), 584–595.

384   [20] G. Trtnik, M. Gams, The use of frequency spectrum of ultrasonic P-waves

385   to monitor the setting process of cement pastes, Cem. Concr. Res. 43

386   (2013), 1–11.

387   [21] ASTM C31 / C31M-15ae1, Standard Practice for Making and Curing

388   Concrete Test Specimens in the Field, ASTM International, West

389   Conshohocken, PA, 2015

390   [22] P. Duhamel, M. Vetterli, Fast fourier transforms: A tutorial review and a

391   state of the art, Signal Processing 19 (1990), 259-299.

392   [23] ASTM C39/C39M-16 Standard Test Method for Compressive Strength of

393   Cylindrical Concrete Specimens, ASTM International, West Conshohocken,

394   PA, 2016

395   [24] P. Anugonda, J. S. Wiehn, J. A. Turner, Diffusion of ultrasound in concrete,

396   Ultrasonics 39 (2001), 429–435.

397   [25] A. Villarreal, S. Solis-Najera, L. Medina-Gómez, Application of Waterman-

398   Truell and the Dynamic Generalized Self-consistent Models on Concrete,

399   Physics Procedia 70 (2015), 437 – 441.

400   [26] J. F. Chaix, V. Garnier, G. Corneloup, Ultrasonic wave propagation in

401   heterogeneous solid media: Theoretical analysis and experimental

402   validation, Ultrasonics 44 (2006), 200–210.

403   [27] V. M. Malhotra, N. J. Carino, Handbook on Nondestructive Testing of

404   Concrete, second ed., CRC press, Washington, D.C., 2003.

405   [28]   T. Parenta, N. Domedea, A. Selliera, L. Mouattb, Mechanical

406   characterization of limestone from sound velocity measurement, Int. J. of

407   Rock Mech. & Min. Sci. 79 (2015), 149–156.

408   [29] I. Fischer, B. Pichler, E. Lach, C. Terner, E. Barraud, F. Britzb,

409   Compressive strength of cement paste as a function of loading rate:

410   Experiments and engineering mechanics analysis, Cem. Concr. Res. 58

411   (2014), 186–200.

412   [30]   C. Kohlhauser, C. Hellmich, Ultrasonic contact pulse transmission for

413   elastic wave velocity and stiffness determination: Influence of specimen

414   geometry and porosity, Eng. Struct. 47 (2013), 115–133.

415   [31]   B. C. Kim, J. Y. Kim, Characterization of ultrasonic properties of concrete,

416   Mech. Res. Commun. 36 (2009), 207–214.

417   [32]   J. Berriman, P. Purnell, D.A. Hutchins, A. Neild, Humidity and aggregate

418   content correction factors for air-coupled ultrasonic evaluation of concrete,

419   Ultrasonics 43 (2005), 211–217.

420   [33]   S. A. Abo-Qudais, Effect of concrete mixing parameters on propagation of

421   ultrasonic waves, Constr. Build. Mater. 19 (2005), 257-261.

422

423

424

425

426

427

428

429

430

431

432

433

434

Figure captions

435 **Figure captions**

436 Fig 1. Evolution of concrete compressive strength (blue triangle) and saturated density

437 (green squares) versus age of concrete w/c = 0.60.

438 Fig. 2. Frequencies versus testing age for (a) aggregate and (b) cement paste. The

439 transducers used were 100 kHz longitudinal wave.

440 Fig. 3. Frequencies versus testing age for (a) aggregate and (b) cement paste. The

441 transducers used were 100 kHz transversal wave.

442 Fig. 4. Frequencies versus testing age for (a) aggregate and (b) cement paste. The

443 transducers used were 250 kHz longitudinal wave.

444 Fig. 5. Frequencies versus testing age for (a) aggregate and (b) cement paste. The

445 transducers used were 250 kHz transversal wave.

446 Fig. 6. Evolution in time of energies associated with cement paste and aggregates versus

447 testing age for transversal wave transducers (a) 50 kHz, (b) 100 kHz, (c) 180 kHz, (d)

448 250 kHz and (e) 500 kHz

449 Fig. 7. Evolution in time of energies associated with cement paste and aggregates versus

450 testing age for longitudinal wave transducers (a) 100 kHz, (b) 250 kHz and (c) 500 kHz

451 Fig. 8. Attenuation related to cement paste and aggregates energy bands, for (a)

452 transversal and (b) longitudinal wave transducers
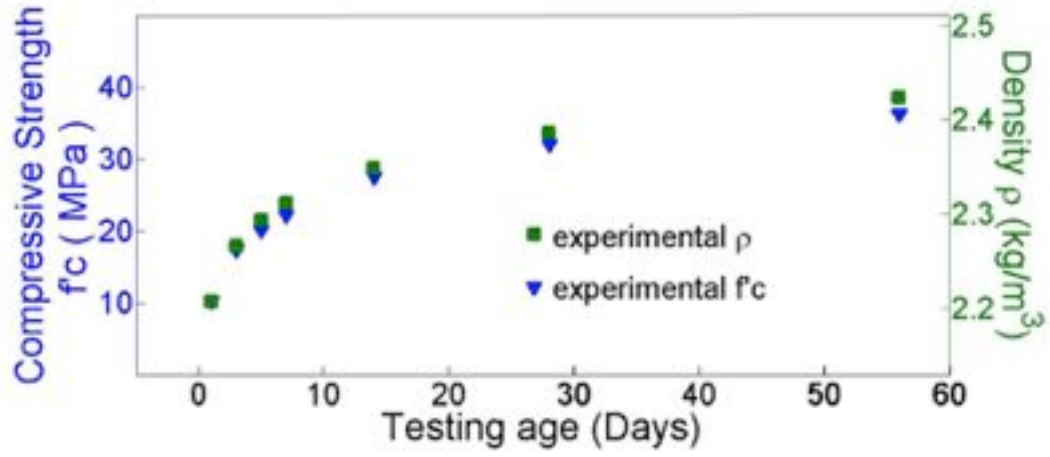
453

454

455

456

457

458

459

Fig 1.
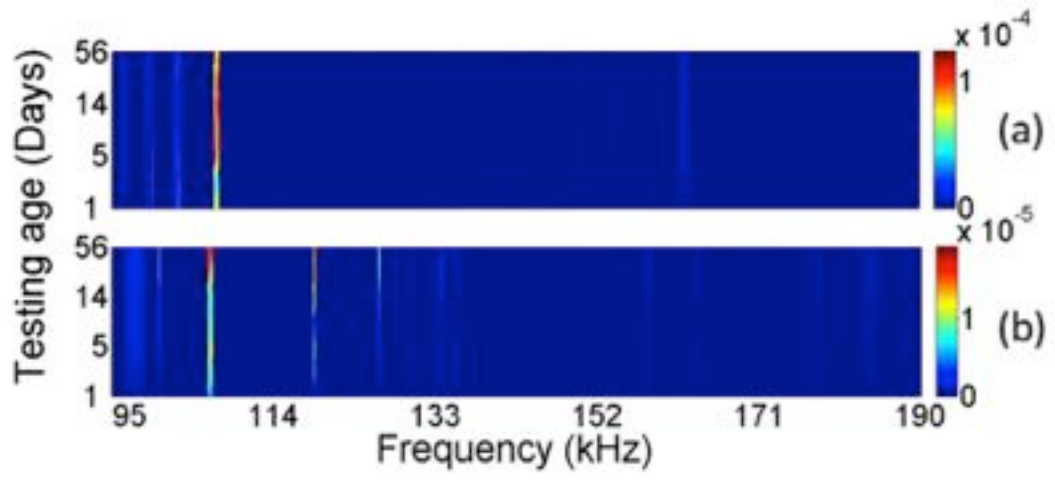
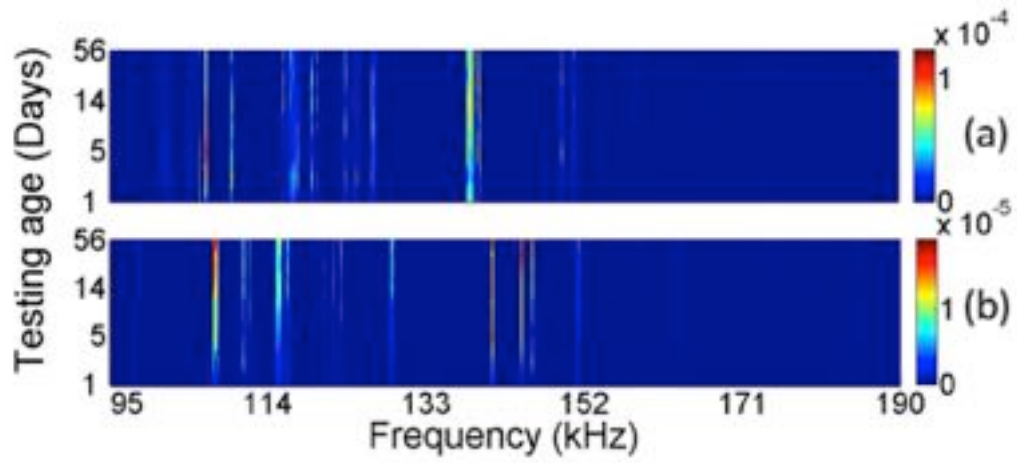Fig. 2.

Fig. 3.

498
499
500
501
502
503
504
505
506
507
508
509
510
511
512
513
514
515
516
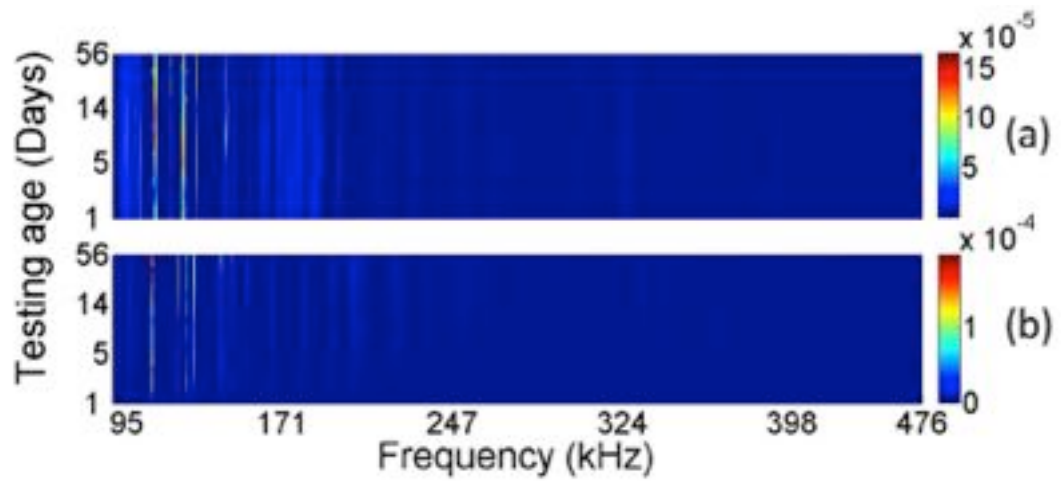
Fig. 4.

517

518

519

520

521

522

523

524

525

526

527

528

529

530

531

532

533

534

535
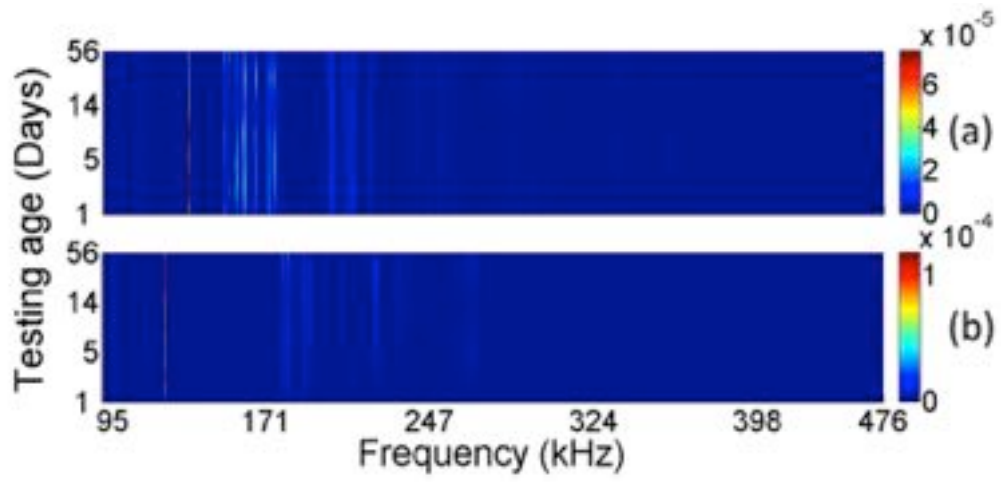
Fig. 5.

(a)

(b)

(c)

(d)

(e)

555
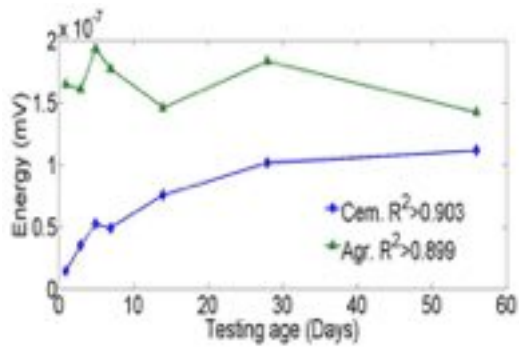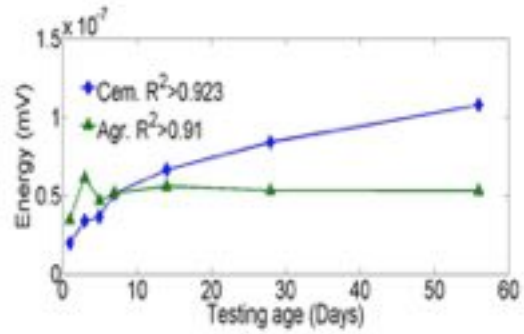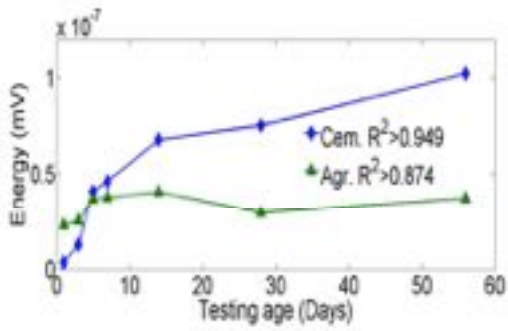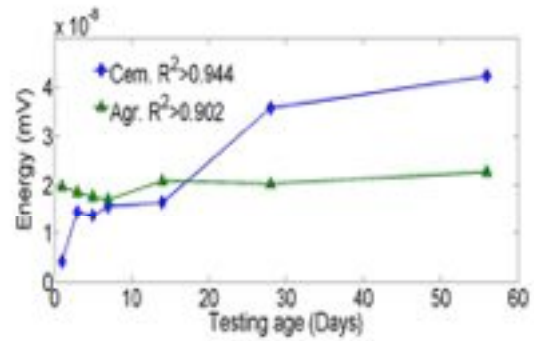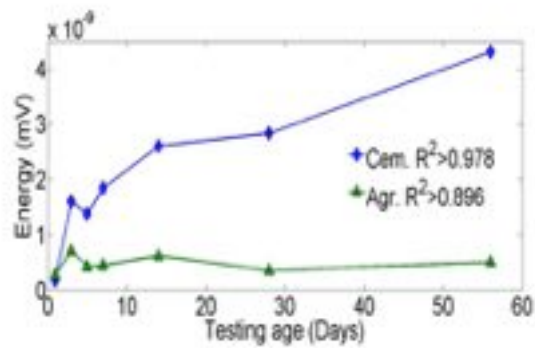
556   Fig. 6.

557

558

559

560

561

562

563   Fig. 7.
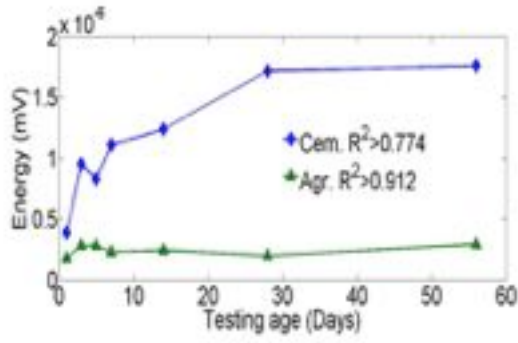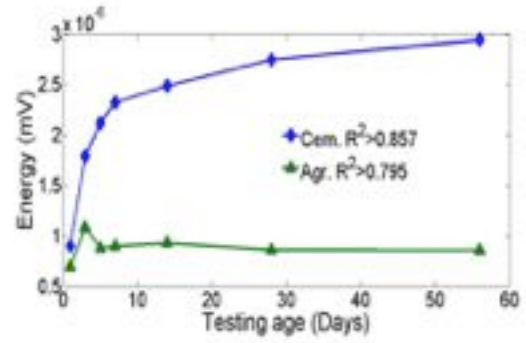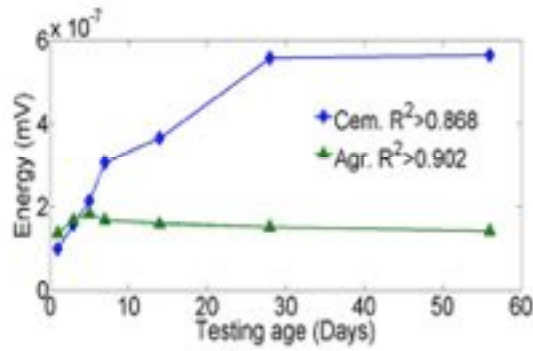
564

565

566

567

568

569

570

571

572

573

574
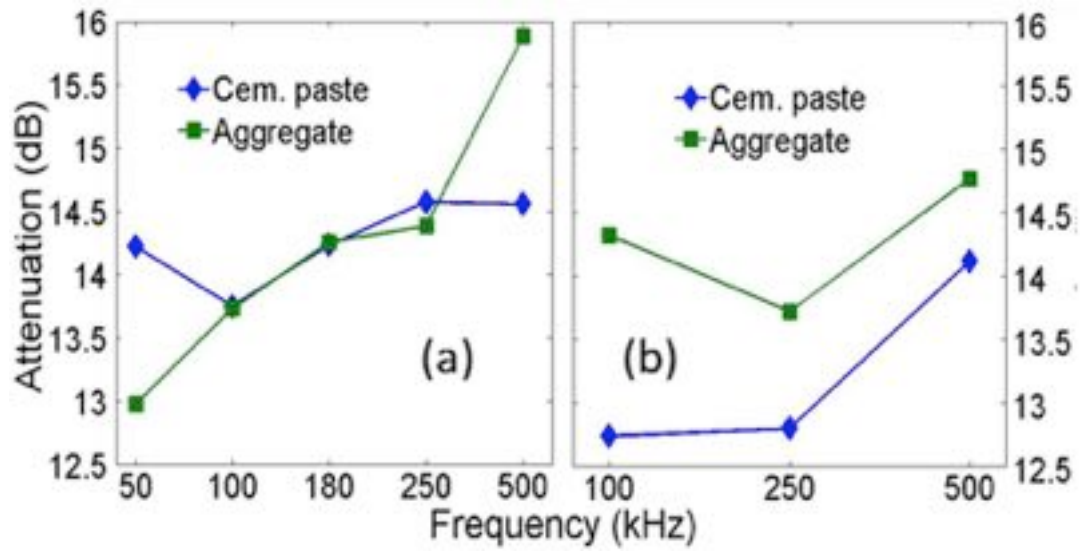
Fig. 8.

575

576

577

578

579

580

581

582

583

584

585

586

587

588

589

590

591

592

593   Table 1. Chemical composition of main oxides for the Ordinary Portland Cement (OPC)

594   used.

Main oxides components	%
SiO_2	21.1
Al_2O_3	3.7
Fe_2O_3	4.5
CaO	61.9
MgO	1.8
K_2O	0.3
Na_2O	0.1
SO_3	1

595

596

597

598

599

600

601

602

603

604

605

606

607

608

609   Table 2. Wavelengths generated by the time-evolution of specimens, using the ultrasonic

610   pulse velocity of each transducer

Transducer frequency (kHz)	Transducer diameter (D) (mm)	wavelength at day 1 (λ) (mm)	wavelength at day 56 (λ) (mm)	Mean $\pm$ std dev wavelength (λ_M) (mm)	Radiation pattern $\beta = \dfrac{D}{\lambda_M}$
Transversal wave transducer					
50	42	53.2	60.0	56.9 $\pm$ 2.29	0.7
100	29	21.6	25.7	24.2 $\pm$ 1.56	1.2
180	42	13.7	13.5	13.6 $\pm$ 0.13	3.1
250	29	6.5	7.8	7.3 $\pm$ 0.42	4.0
500	29	3.2	3.8	3.6 $\pm$ 0.21	8.1
Longitudinal wave transducer					
100	42	22.5	28.5	25.5 $\pm$ 2.19	1.6
250	42	15.5	19.1	17.4 $\pm$ 1.51	2.4
500	29	7.3	10.1	9 $\pm$ 0.95	3.2

611

612

613

614

615

616

617

618

619

620   Appendix A

621   Fig. 9. Frequencies versus testing age for (a) aggregate and (b) cement paste. The

622   transducers used were 50 kHz transversal wave.

623   Fig. 10. Frequencies versus testing age for (a) aggregate and (b) cement paste. The

624   transducers used were 180 kHz transversal wave.

625   Fig. 11. Frequencies versus testing age for (a) aggregate and (b) cement paste. The

626   transducers used were 500 kHz longitudinal wave.

627   Fig. 12. Frequencies versus testing age for (a) aggregate and (b) cement paste. The

628   transducers used were 500 kHz transversal wave.

629

630

631

632

633

634

635

636

637

638

639

640

641

642

643

644
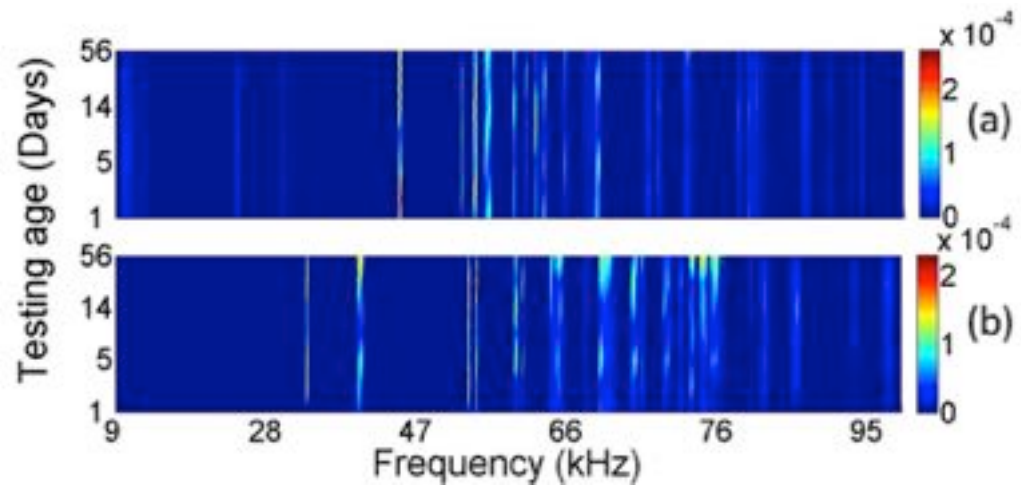
Fig. 9.

Fig. 10.

Fig. 11.

702
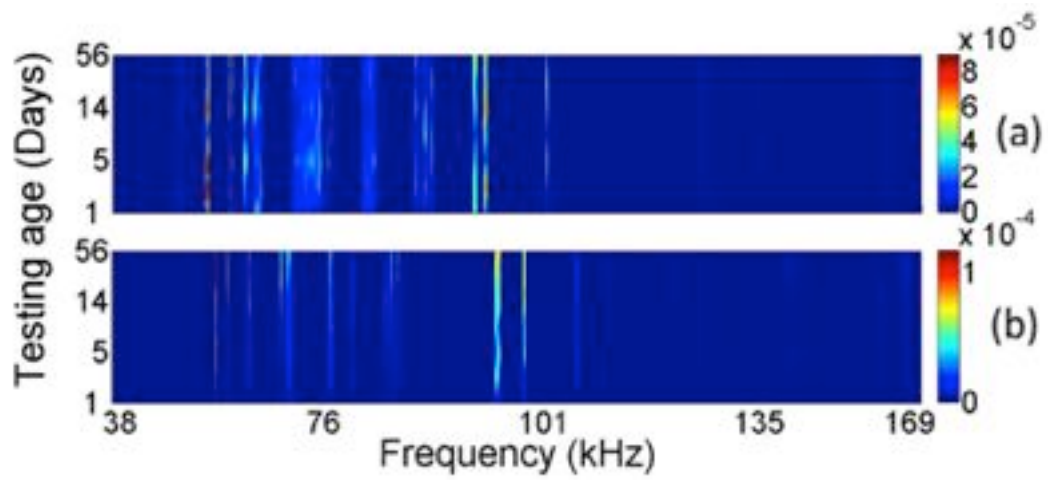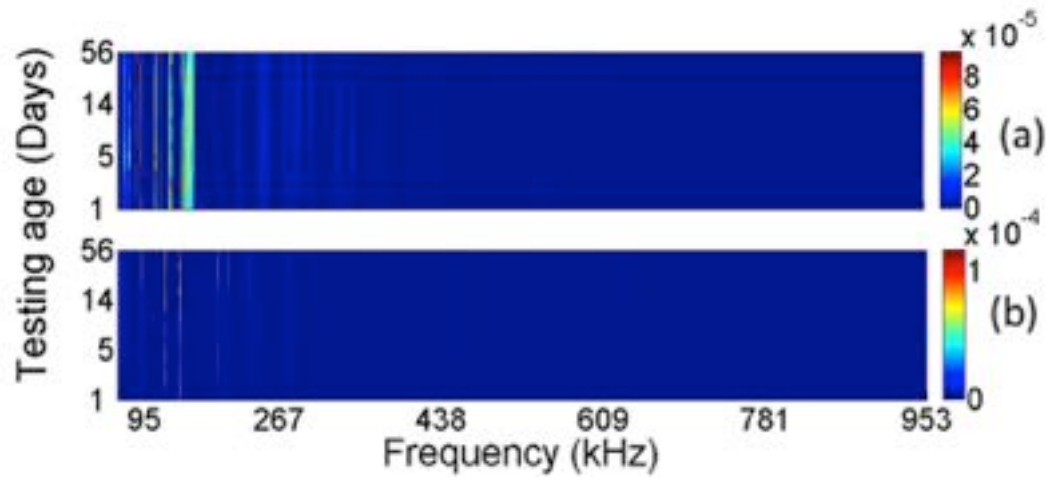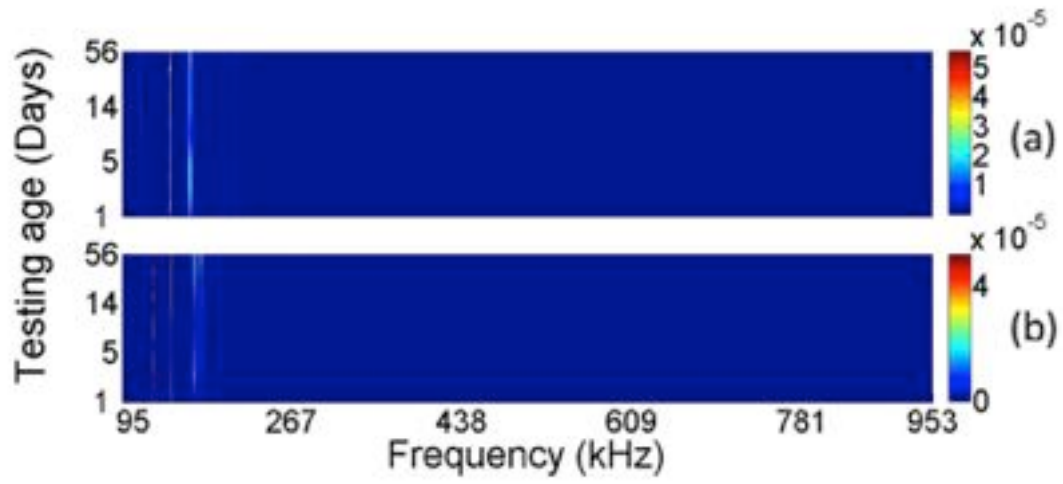
703   Fig. 12.

Capítulo II

Non-destructive ultrasound based cement paste carbonation index

Mario F. Cosmes-López[1], Francisco Castellanos[2*], Prisciliano F. de J. Cano-Barrita[2], Frank M. León-Martínez[2]

[1] *PhD student at Instituto Politecnico Nacional, CIIDIR Unidad Oaxaca, Hornos No. 1003, Santa Cruz Xoxocotlán, Oaxaca, Mexico, C.P. 71230.*

[2] *Researcher at Instituto Politecnico Nacional, CIIDIR Unidad Oaxaca, Hornos No. 1003, Santa Cruz Xoxocotlán, Oaxaca, Mexico, C.P. 71230.*

Phone: + 52 951 5170610, Emails: mcosmesl1200@alumno.ipn.mx, fcastellanos@ipn.mx, pcano@ipn.mx and fmleonm@ipn.mx

*Corresponding author

Abstract

18   This study presents a new method to assess the degree of carbonation in cement paste specimens,

19   by analyzing their ultrasound response to different excitation frequencies. Eighteen cylindrical

20   cement paste specimens measuring 50 mm in diameter and 57 mm in height were cast with three

21   different water to cement ratios (w/c = 0.60, 0.50 and 0.40). The samples were moist cured for

22   four months to reach a high degree of hydration. Then the samples were conditioned in an

23   environmental chamber at 30 ^{o}C and 65 % relative humidity. After obtaining constant mass, each

24   specimen was coated with epoxy resin on the curved surface, one circular face was covered with

25   parafilm. The specimens were then exposed to accelerated carbonation in an environmental

26   chamber at 30 ^{o}C, 65 % relative humidity, and 4 % CO_2 (v/v). One control specimen was kept at

27   the same environmental conditions of temperature and relative humidity, without CO_2. All the

28   specimens were tested at 1, 3, 5, 7, 14, 28 and 56 days, during carbonation process, using

29   longitudinal and transversal ultrasonic waves with frequencies ranging from 100 kHz to 500

30   kHz. Assuming the carbonation in cement paste causes changes in the frequencies spectrum as

31   the carbonation front progresses, causing important changes on porosity and pore structure of the

32   cement paste. By analyzing these changes, we may infer the degree of carbonation in the

33   specimen. Results show that it was possible to assess the degree of carbonation of cement paste

34   specimens by frequency domain analysis as a function of carbonation time, regardless of the

35   water to cement ratio.

36   **Keywords:** ultrasound analysis; carbonation; cement paste; Fourier analysis; carbonation

37   index

1. Introduction

The alkaline pore solution of the hydrated cement paste protects the reinforcing steel from corrosion caused by carbonation [1,2]. Carbonation is the result of the reaction between CO_2 from the environment and the main hydration products such as calcium hydroxide and CSH in the presence of moisture, generating calcium carbonate and silica gel [3]. As a result, the pH of the pore solution is reduced from above 12.5 to less than 9. This may destroy the passivating layer on the steel and corrosion starts [4]. Carbonation not only affects the chemistry of the pore solution, but also affects the porosity and pore size distribution of the cement paste [5]. In some cases, the porosity is reduced and the strength is increased. In other cases, the porosity is increased, especially when using fly ash [6].

Penetration of CO_2 is function of the permeability of hardened cement paste in concrete, as well as the CO_2 concentration and environmental factors such as temperature and relative humidity [7]. The carbonation front follows the square root of time behavior. Regarding the environmental factors, the penetration is strongly influenced by the concentration of CO_2, temperature and relative humidity [8]. Therefore, conclusions based on accelerated carbonation tests, can be used to estimate the service life of reinforced concrete structures [6, 9].

The most common and simple technique used to measure the carbonation depth is by spraying a phenolphthalein indicator on a freshly broken surface. However, it is destructive in nature and in addition it underestimates the carbonation front penetration [10]. Other destructive methods such as the thermogravimetric analysis (TGA), X-Ray diffraction and Fourier transformation infrared spectroscopy (FTIR) have been also used to detect the changes in concrete produced by

59 carbonation [11,12,13]. The gammadensimetry [14] is able to measure the total penetration of the

60 CO_2 during laboratory accelerated tests. However, in order to obtain a full picture of the

61 carbonation process numerous samples need to be tested.

62 Transmission wave velocity and wave attenuation are affected by the density and the elastic

63 modulus of materials [15,16], which makes ultrasound wave analysis a potential technique for

64 assessing carbonation of the cement paste. This article presents a new approach on the analysis

65 of ultrasound signals to study carbonation of mature cement paste specimens with different w/c

66 ratios. This approach was adapted from our methodology proposed for distinction of aggregate

67 and cement paste in concrete samples from analysis of ultrasound signals [17].

2. Experimental procedure

68

2.1. Materials

69

70 Mexican ordinary Portland cement class 30RS (ASTM C150 Type I) was used. A total of 18

71 cylindrical cement paste specimens measuring 50 mm in diameter and 57 mm in height were cast

72 with three different w/c ratios of 0.60, 0.50 and 0.40. After one day, the specimens were stripped

73 and moist cured in a saturated lime solution at 40 ± 2 °C for four months, according to the

74 ASTM C31 [18]. Then the specimens were stabilized in an environmental chamber at 30 °C and

75 65 % relative humidity, until constant mass was achieved.

76 After stabilization, each specimen was coated with epoxy resin on the curved surface. Before

77 carbonation commenced, one circular face was covered with paraffin film to expose only one

78 face to CO_2 penetration. Five specimens of each w/c ratio were exposed to accelerated

79 carbonation in an environmental chamber at 30 ºC, 65 % relative humidity, and 4 % CO_2 (v/v).

80 One control specimen was kept at the same temperature and relative humidity, without CO_2.

81 **2.2. Method**

82 **2.2.1. Ultrasonic measurements**

83 Six specimens were tested at ages of 1, 3, 5, 7, 14, 28 and 56 days, after beginning the

84 carbonation process. For each test, the ends of each specimen were covered with paraffin film

85 and heated with a heat gun for 60 seconds in order to obtain a smooth thin layer, which prevented

86 penetration of the coupling agent (petroleum jelly) into the specimen. The excitation signal was

87 generated by a 5077PR pulser/receiver with a voltage of 200 V and a variable factor of electronic

88 damping or gain depending on the amplitude of the received signal. A record was maintained of

89 their responses in through-transmission with longitudinal and transversal ultrasonic waves,

90 generated by transducers with frequencies ranging from 100 kHz to 500 kHz. The position of the

91 transducers and their applied pressure were kept constant during the experiment.

92 **2.2.2. FTIR measurements**

93 Three specimens of each w/c ratio were taken at 1, 3, 5, 7, 14, 28 and 56 days, for carbonated

94 and control specimens. Once the epoxy resin coat was removed, the cement paste samples were

95 crushed with hammer and chisel and then the small pieces were ground with an agate mortar.

96 The fine powder obtained was sieved by the No. 100 mesh (150 μm), then oven-dried at 105 ° C

97 for 24 hours, and finally stored in sealed bags. The bags were inside a desiccator with silica gel

98 and soda lime at room temperature, to avoid moisture adsorption and carbonation of the powder

99 samples until FTIR measurements were performed [13].

100 Three different FTIR spectra of each powder sample were taken with a ThermoScientific

101 instrument Model Nicolet 6700 (ThermoScientific, MA, USA) and the mean value of the area

102 under the curve was calculated for the vibration bands at 1418 cm^{-1} and 872 cm^{-1} corresponding

103 asymmetric stretching and out plane bending for the carbonate ion in the $CaCO_3$. The initial

104 amount of $CaCO_3$ in the anhydrous cement (3%) was determined by thermogravimetric analysis

105 and this value was related to the area under the curve of the bands corresponding to $CaCO_3$ in the

106 FTIR spectrum. This served as a basis for estimation of the amount of $CaCO_3$ by weight in the

107 carbonated samples.

3. Wave analysis

3.1. Signal processing

110 The method proposed for analysis of the ultrasound signals was intended to assess the degree of

111 carbonation in cement pastes with different w/c ratios. The main feature exploited by the

112 proposed method was that the CO_2 penetration affects the microstructure of the cement paste by

113 generating of calcium carbonate, and the consequent modification of its density and physical

114 properties [19]. Assuming that the degree of hydration [20] of the cement pastes was high

115 because of the relatively long moist curing time, it was feasible to consider that variations in the

116 ultrasonic response of cement pastes will be a result of carbonation, as opposed to the invariant

117 behavior of the control specimens.

118 This analysis methodology was based on our previous work [17]. The first step in the proposed

119 analysis was to calculate the time-discrete Fourier Transform (TDFT) of the ultrasound signal

120    $f(n\Delta t)$, according to Eq. (1). The Fast Fourier Transform (FFT) is a standard signal processing

121   technique for analyzing ultrasound signals [21].

122    $F(k\Delta\omega) = \frac{1}{2\pi}\sum_n f(n\Delta t)e^{-i(2\pi kn/N)}\Delta t$ (1)

123   where T is the duration of the ultrasound signal, discretized at a sampling rate Δt=T/N, and kΔw

124   are the resulting discrete frequencies.

125   A window of F(k$\Delta\omega$) was subsequently selected from the frequency response function of the

126   transducers with an intensity greater or equal to 6 dB, as specified by the ultrasound transducer

127   manufacturer.

128    $G(k\Delta\omega) = \begin{cases} F(k\Delta\omega), & k_1 \leq k \leq k_2 \\ 0, & elsewhere \end{cases}$ (2)

129   The changes over time of the seven spectra obtained (1, 3, 5, 7, 14, 28 and 56 days) from

130   ultrasound measurements $G_i(k\Delta\omega)$, where $1 \leq i \leq 7$, was analyzed for the identification of the

131   carbonation process. This analysis consists of the correlation of variations along time of every

132   frequency amplitude $|G_i(k\Delta\omega)|$, with a constant function. For the identification of frequencies k_c

133   related to the carbonated cement paste. The correlation was made from the first two testing days,

134   until the eighth day, obtaining seven sets of correlations for each specimen.

135   A histogram was obtained for each of the seven sets of correlations. The abscissa x was

136   discretized by class and associated to each correlation coefficient, for each of the seven sets of

137   correlations. The ordinate represents the number of frequencies in each class. The size of the

138   class was chosen with a precision of 0.001. In order to improve understanding of the data

48

139   behavior, the histogram obtained was duplicated using a function which satisfies the next

140   condition:

141    $H(x) = H(2 - x)$ (3)

142   Such that the function obtained is defined as follows:

143    $K(x) = \begin{cases} H(x), & 0 \leq x \leq 1 \\ H(2 - x), & 1 < x \leq 2 \end{cases}$ (4)

144   Then, the resulting signal was adjusted to a normal distribution function, minimizing the squared

145   error, as shown in Figure 1.

146    $I_a(x) = \beta\, e^{-\left(\frac{x-1}{\sigma}\right)^2}$ (5)

147
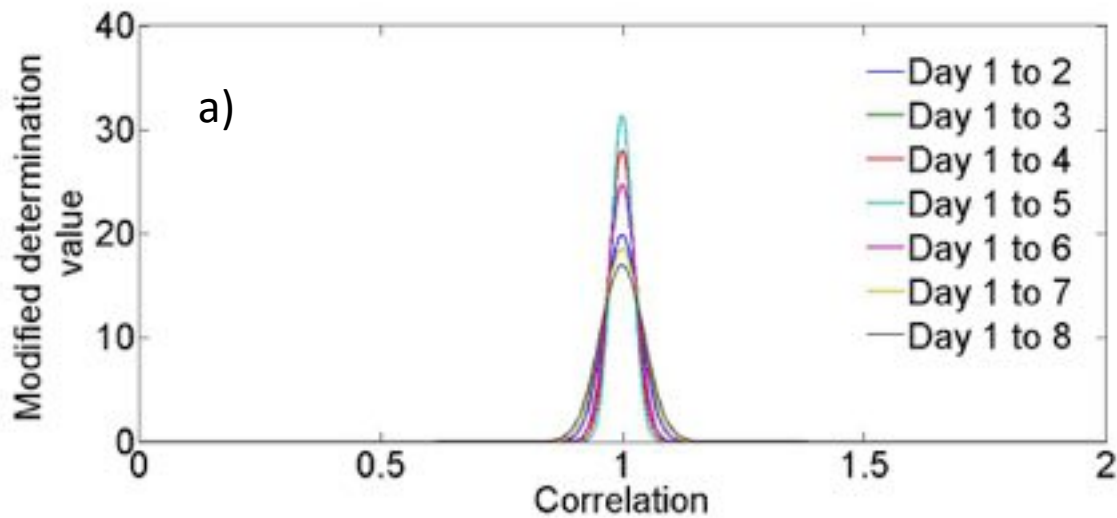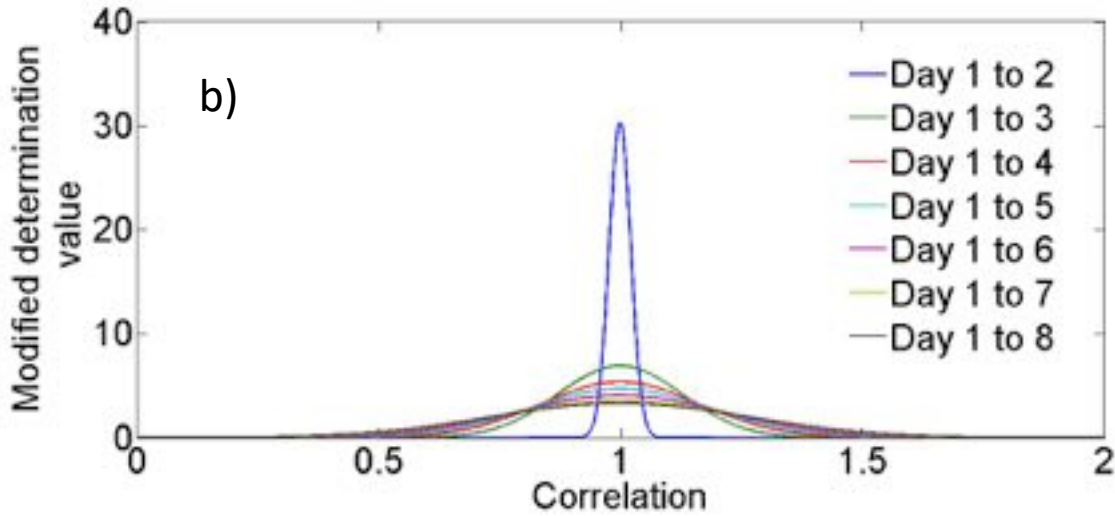
Figure 1 Normal distribution adjustment of the accumulative data for each measurement day, of control (a) and carbonated (b) specimen, for the water to cement ratio of 0.50 using the longitudinal wave transducer of 100 kHz.

This process was performed for each of the seven set of correlations. Using the inverse of the amplitude β, the index I was obtained as follows.

$$I = \frac{(^W/_C)*\gamma}{\beta} \tag{6}$$

where I is the carbonation index, dependent on the $^W/_C$ and the empirical obtained factor γ, that may be linked to exposure conditions.

In previous studies, it was found that the exposure to high concentration of CO_2 cause a degradation of the calcium silicate hydrate (C-S-H), weakening the cement matrix which will generate cracks through the specimens, being more evident with higher water/cement ratios [5].

160   Since the generation of cracks is highly probable when the cement paste is carbonated, as the

161   products generated by the carbonation reaction occupy a higher volume than the hydration

162   products [22, 23]. For this reason, it was necessary to correct the previous index by attenuation A

163   using the following equation.

164    $$A = -\log\left(\frac{A_E}{A_S}\right) \qquad\qquad (7)$$

165   where A_E is the amplitude of the first measurement day and A_S is the amplitude of the

166   subsequent measurement days.

167   The correction by attenuation Eq. (7) of the index obtained in Eq. (6), produces the index I_A for

168   the carbonation of the cement paste was obtained as:

169    $$I_A = I - A \qquad\qquad (8)$$

170   **3.2. Wavelength**

171   The wavelength λ depends on wave velocity (UPV) and transducer frequency (Ω) according to

172   Eq. (9).

173    $$\lambda = \frac{UPV}{\Omega} \qquad\qquad (9)$$

174   The sensitivity to detect defects/changes in the cement paste was given by the relation between

175   the size of the defect/changes and the wavelength [24]. The sensitivity depends on the transducer

176   frequency, which increase directly proportional to the frequency employed, assuming constant

177 UPV [25]. In carbonated specimens, different degrees of carbonation may be detected depending

178 on the frequency transducers used.

4. Results and discussion

179

4.1. Ultrasound pulse velocity

180

181 The first analysis of the data was calculating the ultrasound pulse velocity (UPV). In Figure 2 it

182 is shown the evolution in time of the UPV for all the specimens with three different w/c ratios.

183 The UPV allows only distinction between the different w/c ratio employed, but not for the

184 difference between control and carbonated specimens.

185 As can be seen, the standard error of the UPV for the w/c = 0.50 and 0.60 was higher in

186 comparison with that of the w/c = 0.40. This effect may be due to the generation of cracks caused

187 by the carbonation process which was higher for the w/c = 0.50 and 0.60. In the case of the w/c =

188 0.40 showed an increase of the UPV after 30 days of CO_2 exposure, influenced by the attack of

189 C-S-H and CH producing important changes in the elastic modulus and density, despite of the

190 short carbonation front.

191
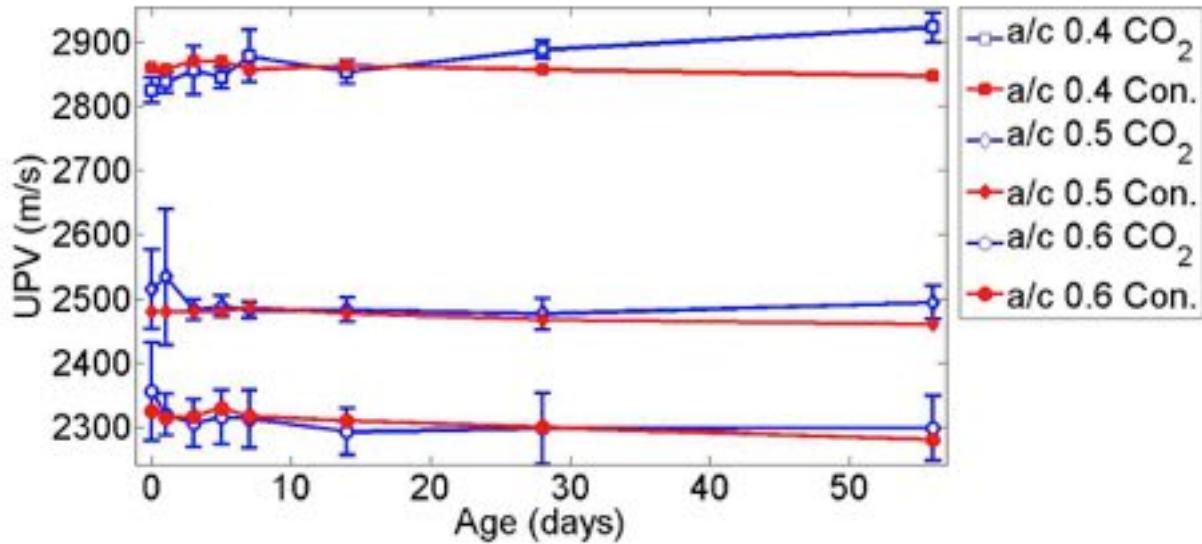
Figure 2. Evolution in time of the UPV versus testing age for control (red lines) and carbonated

(blue lines) specimens for water/cement ratios of 0.40 (square), 0.50 (diamonds) and 0.60

(circles). The error bars represent one standard deviation.

Results from ultrasound testing were compared with the content of calcium carbonate ($CaCO_3$)

estimated by the Fourier Transform Infrared Spectroscopy (FTIR) measurements [13], presented

in the following section.

4.2. Carbonation index

Variations in the porosity and pore structure of cement pastes caused by carbonation depend on

the properties of the cement paste and the exposure environmental conditions [19, 27]. Three w/c

ratios (0.40, 0.50 and 0.60) were analyzed for indexing the degree of carbonation in cement

pastes whose results are shown in Figures 3-5.

203   It was expected that the progressive changes caused by the carbonation process, gradually

204   modify the cement paste microstructure. These variations slowly affect the frequency of the

205   ultrasound response. This effect distinguishes the control from the carbonated specimens.

4.2.1. Cement paste samples with water/cement ratio of 0.60

207   Figure 3 shows the results of the ultrasonic measurements for the control and carbonated

208   specimens for cement paste with w/c ratio of 0.60. Figure 3a shows the evolution over time of

209   the carbonation index for the control and carbonated specimen tested with 100 kHz longitudinal

210   wave transducers. The behavior between both types of specimens was similar, although the trend

211   of the carbonation index had a strong correlation with the FTIR data. The behavior of the control

212   specimen may be explained by the stabilization process which cause drying shrinkage and

213   cracking of the cement paste [28]. This was reflected in variations of the ultrasound response of

214   the control specimens during the measurements as had been seen in previous studies [29,25].

215   This effect was present in the rest of the measurements with other transducers, as can be seen in

216   Figures 3b-e, but with less impact in the index response due to the variations in wavelength

217   calculated in Table 1 [30].

218   In Figures 3b and 3d, measurements with the 100 kHz and 250 kHz transversal wave transducers,

219   respectively, had a weak correlation with the FTIR data. The former correlation was mostly

220   caused by the cracking and porosity of the specimens with a high w/c ratio [19]. These factors

221   had a high impact on the propagation of transversal waves, making it difficult to assess the

222   carbonation penetration, since they cannot propagate through fluids (water and air) [31].

223 Figure 3c shows the measurements with the 250 kHz longitudinal wave transducers. The control

224 specimens keep a behavior almost constant in contrast with the index of the carbonated specimen

225 whose values increase. The correlation between the carbonation index proposed and the FTIR

226 data was strong. Although, the correlation was weaker than that obtained with the 100 kHz

227 longitudinal wave transducers, in this case, it was possible to distinguish between the behavior of

228 the control and the carbonated specimen. This distinction was possible due to the changes in

229 wavelength and in the propagation properties of this kind of waves (Table 1) which can travel

230 through solids and fluids [32].

231 Measurements with the 500 kHz longitudinal wave transducers are shown in Figure 3e. The

232 distinction between control and carbonated specimen behavior was easier, in comparison with

233 the results of the other transducers. Also, the carbonation index had the strongest correlation with

234 the FTIR data and the dispersion of the carbonation specimens was the lowest. The wavelength

235 and the propagation properties of the longitudinal waves of these transducers [33], as shown in

236 Table 1, improves tracking of the carbonation process. Furthermore, the final value of the

237 carbonation index proposed was close to the one obtained with FTIR. However, the losses of

238 energy are so high that causes underestimation of carbonation degree.
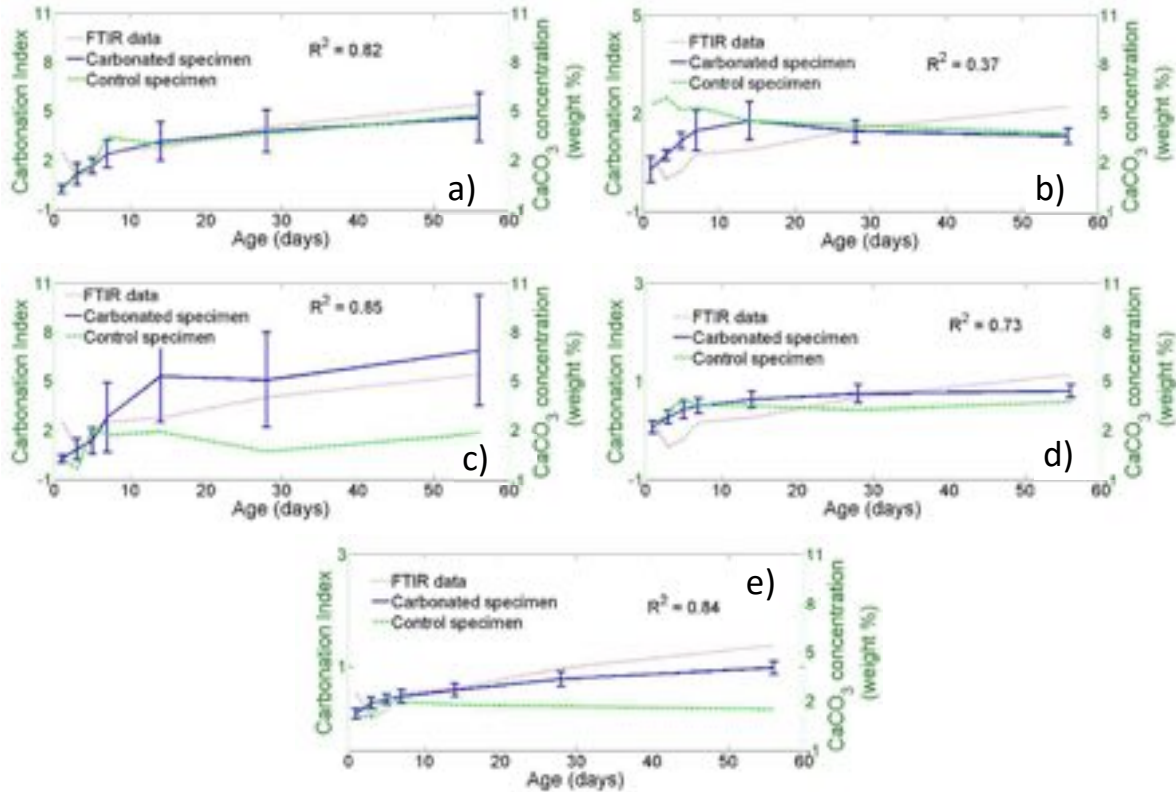
Figure 3. Evolution of carbonation index and content of calcium carbonate by FTIR, versus testing age for longitudinal wave transducers of 100 kHz (a), 250 kHz (c), 500 kHz (e) and transversal wave transducers of 100 kHz (b), 250 kHz (d), for cement paste specimens with w/c ratio = 0.60.

Table 1 shows how the wavelength of the carbonated specimens was lower than the control samples, which is explained by the density increase due to generation of calcium carbonate ($CaCO_3$), for the same frequency of the transducers. As the transducer frequency increases, the wavelength decreases enhancing the sensitivity of the ultrasound signals, along with reducing the standard deviation between specimens. Also, a small decrease between the same frequency transducers but different wave type is produced; this decrease was more visible in carbonated specimens.

251 Table 1. Mean and standard deviation of the wavelengths generated by the time-evolution of

252 control and carbonated specimens with w/c=0.6

Frequency (kHz)	Diameter of Transducer (D) (mm)	Control wavelength (λ) (mm)		Carbonated wavelength (λ) (mm)	
		Mean ($M_{\lambda Co}$)	Std dev	Mean ($M_{\lambda Ca}$)	Std dev
Longitudinal wave transducer					
100	42	23.13	0.47	23.12	0.15
250	42	9.38	0.31	9.28	0.08
500	29	4.74	0.17	4.68	0.04
Transversal wave transducer					
100	29	22.56	0.66	22.33	0.17
250	29	9.35	0.34	9.21	0.09

253

254 4.2.2. Cement paste samples with water/cement ratio of 0.50

255 Figure 4 shows the results of the ultrasonic measurements for the control and carbonated

256 specimens with a w/c ratio of 0.50. The results of the ultrasound measurements with the 100 kHz

257 transversal wave transducer are shown in Figure 4b. Although, the correlation with the FTIR data

258 was weak, the distinction between the control and the carbonated specimens was possible. This

259 was because of the slow penetration of CO_2, result of the lower permeability of this paste

260 compared with the permeability of the paste with w/c = 0.60 [34].

261 This decrease in the carbonation ratio allows a slower formation of the $CaCO_3$, enlarging the

262 time of occurrence of the structural changes in the cement paste [19]. These smooth the process

263 of carbonation allowing a better assess of the changes in the cement matrix and therefore a better

264 studied of the specimen, which was reflected in the stronger correlation of the carbonation index

265 for all transducers, in comparison with the cement paste of 0.60. In the case of Figures 4a, 4c, 4d,

266 and 4e, the correlation with the FTIR data becomes stronger as the transducer frequency

267 increases. This behavior was related to the gain in sensitivity due to the decrease of the

268 wavelength as the transducer frequency increases, as shown in Table 2.

269 Figure 4a shows the evolution in time of the carbonation index for the 100 kHz longitudinal

270 wave transducers. It was possible to distinguish the behavior between the control and the

271 carbonated cement paste specimens. The correlation was stronger than the 100 kHz transversal

272 wave transducer, which might be explained by fewer losses of the signal energy by cracks, void

273 and water caused by the carbonation process [6]. Nevertheless, the standard error of the data was

274 higher than the ones of Figures 4c, 4d and 4e.

275 The correlation obtained by the 250 kHz longitudinal wave transducer was the strongest on

276 evaluating the 0.5 w/c cement paste, as shown in Figure 4c. The rise of the correlation was

277 mostly caused by the decrease of the wavelength and the property of the longitudinal waves to

278 travel through different media, as shown in Table 2. This causes less energy losses due to the

279 specimen heterogeneities with better interaction during the measurements, but increasing the

280 standard error between the carbonation index for different specimens, as well as the sensitivity.

281 The results for the 250 kHz transversal wave transducer are shown in Figure 4d. The stronger

282 correlation, compared with the 100 kHz transversal wave transducer, was due to the lower

283 wavelength. However, the sensitivity was not enough to surpass the correlation of higher or

284 equal longitudinal wave transducers frequency. Although, the preference of the transversal waves

285 to propagate through solids and the slower generation of the solid phases ($CaCO_2$) of the

286 carbonation process had high impact on the standard error of the carbonation index of different

287 specimen measurements, as seen in Figure 4d.

288   The results for the 500 kHz longitudinal wave transducer are shown in Figure 4e. The correlation

289   with the FTIR data was the second strongest of the transducer measurements, because of the

290   wavelength (Table 2) which allows a better interaction with the specimen recollecting more

291   information of the specimen, also cause a higher loss of energy. As expected, the sensitivity

292   increases with time, but the heterogeneities between different specimens induces a rise of

293   standard error in the carbonation index for different specimens, caused by the heterogeneities

294   produced by the carbonation process.
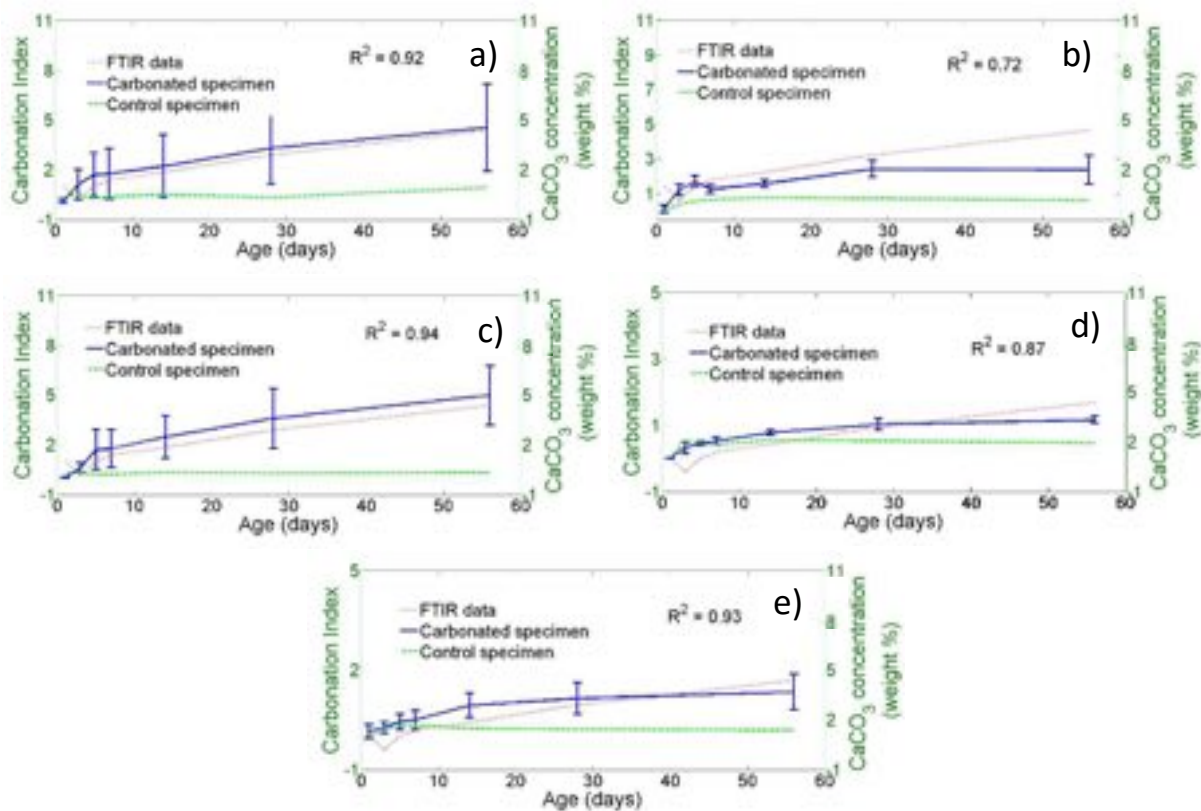
295

296   Figure 4. Evolution of carbonation index and content of calcium carbonate by FTIR, versus

297   testing age for longitudinal wave transducer 100 kHz (a), 250 kHz (c), 500 kHz (e) and

298   transversal transducer 100 kHz (b), 250 kHz (d) for cement paste specimens with w/c ratio =

299   0.50.

300   As stated, the wavelength decreases as the frequency transducer increases, but the wavelength

301   between control and carbonated specimens was very close one to another, regardless of the

302   transducer frequency. This behavior was due to the slower carbonation reaction process. The

303   decrease between the same frequency but different type of wave was more evident with the 100

304   kHz transducers than with the 250 kHz transducers.

305   Table 2. Wavelengths generated by the time-evolution of control and carbonated specimens,

306   using the ultrasonic pulse velocity of each transducer for a water/cement ratio of 0.50.

Frequency (kHz)	Diameter of Transducer (D) (mm)	Control wavelength (λ) (mm)		Carbonated wavelength (λ) (mm)	
		Mean ($M_{\lambda Co}$)	Std dev	Mean ($M_{\lambda Ca}$)	Std dev
Longitudinal wave transducer					
100	42	28.63	0.23	28.60	0.08
250	42	10.08	0.13	9.96	0.06
500	29	5.07	0.03	5.01	0.02
Transversal wave transducer					
100	29	24.16	0.24	24.16	0.13
250	29	10.00	0.16	9.88	0.06

307

4.2.3. Cement paste samples with water / cement ratio of 0.40

309   Figure 5 shows the results of the ultrasonic measurements for the control and carbonated

310   specimens with w/c ratio = 0.4. As can be seen in Figure 5a- 5c, it was difficult to distinguish

311   between control and carbonated specimens for this w/c ratio, neither using longitudinal wave

312   transducers of frequencies of 100 and 250 kHz, nor 100 kHz transversal wave transducers. The

313   behavior observed of the carbonation index was rather constant in comparison with the results of

314   the previous w/c ratio analyzed. Even with the decrease of the wavelength, it cannot be assessed

315   the carbonation degree of the specimens. The lower penetration in these specimens was caused

316   by the porosity reduction and the carbonation reaction on the surface of the specimens which

317   prevent the penetration of CO_2 [19].

318   The correlation gets stronger between the FTIR data and the energy percentage calculated for the

319   250 kHz transversal wave transducer. The formation of solid calcium carbonated in the cement

320   paste produced a higher interaction with the propagation of transversal waves, since they prefer

321   to propagate through solid media [30]. This preference allows the wave for better detection of

322   changes caused by the carbonation process in comparison with the longitudinal wave transducer

323   of the same frequency (even with similar wavelengths, Table 3), enabling the distinction between

324   the control and the carbonated cement paste even if the carbonation was at onset.

325   In Figure 5e, the results of the 500 kHz longitudinal wave transducer are shown. It was possible

326   to distinguish the behavior between the control and the carbonated specimen, since the

327   wavelength was the smallest produced (Table 3). The correlation with the FTIR data was

328   stronger than with the others frequencies [13]. As stated, this was due to the size of the

329   wavelength and also to the interaction of the longitudinal wave with the varying media.

330   However, the standard error of the carbonation index increases with time because of the high

331   sensitivity of the high frequency transducer.

332
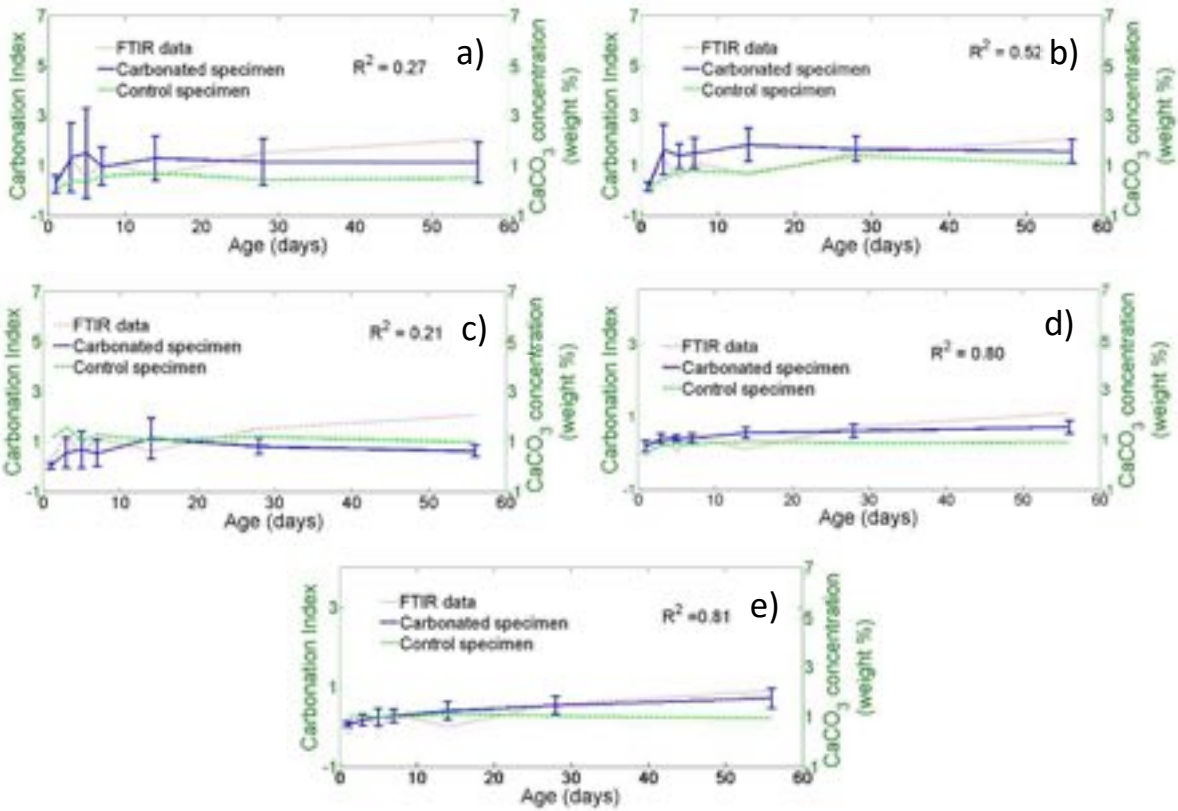
Figure 5. Evolution of carbonation index and content of calcium carbonate by FTIR, versus testing age for longitudinal wave transducer 100 kHz (a), 250 kHz (c), 500 kHz (e) and transversal transducer 100 kHz (b), 250 kHz (d) for cement paste specimens with w/c ratio = 0.40.

Variations in wavelength are shown in Table 3. Although, the wavelength of the control and carbonated specimens was very similar, the small changes in the wavelength are caused by the carbonation process. Also, the wavelength of the different wave type transducers and same frequency are very close one to another.

342 Table 3. Wavelengths generated by the time-evolution of control and carbonates specimens,

343 using the ultrasonic pulse velocity of each transducer for a water/cement ratio of 0.40.

Frequency (kHz)	Diameter of Transducer (D) (mm)	Control wavelength (λ) (mm)		Carbonated wavelength (λ) (mm)	
		Mean ($M_{\lambda Co}$)	Std dev	Mean ($M_{\lambda Ca}$)	Std dev
Longitudinal wave transducer					
100	42	28.63	0.23	28.60	0.08
250	42	11.55	0.07	11.53	0.03
500	29	5.82	0.06	5.83	0.01
Transversal wave transducer					
100	29	27.67	0.20	27.97	0.28
250	29	11.43	0.10	11.50	0.04

344

345 As can be seen in Table 3, the wavelength between the w/c of 0.50 and 0.40 was almost the

346 same, but in the w/c of 0.60, the wavelength was smaller. This was an indicator of the higher

347 porosity of these specimens [24]. The close value of the control wavelength to the carbonated

348 specimen wavelength, can explain the atypical results shown in Figure 3a, compared with the

349 results shown in Figure 4a, where a clear differentiation between carbonated and control

350 specimen can be observed. In the case of Figure 5a, the sensitivity was not enough to

351 differentiate between the control and the carbonated specimen. However, unlike the Figure 3a,

352 both behaviors remained constant, which was an indication that the carbonation front had not

353 advanced enough to be detected and the response behavior seems to be constant, contrary with

354 the results of Figure 3a, where the control specimen had an abnormal behavior.

355 In Figure 3b, the abnormal behavior of the control specimen was even more obvious since the

356 index associated to it had significantly atypical, showing values below zero, which are

357 inconsistent with the rest of the results. In Figure 4b the differentiation between control and

358 carbonated specimen was better than in the rest of the measurements. The increase of the

359   wavelength, observed with the 100 kHz transversal wave transducers, is a parameter that

360   indicates an increasing density of the specimens, with the reduction of the w/c ratio, better than

361   the longitudinal wave transducer of the same frequency, as showed in Table 1-3.

362   Figure 3c, show an improvement in the distinction between the control and carbonated specimen

363   almost as good as Figure 4c, where a clearer distinction between the carbonated and control

364   specimen was possible, compere with Figure 5c. As the transducer frequency employed rise the

365   distinction between the cement past was more clear, as the gap between wavelength increase,

366   being the biggest one among the w/c ratio of 0.6 and 0.4.

367   As can be seen in Figure 4d and 5d, the evaluation of the carbonation improves, even for the w/c

368   ratio of 0.40, which before were unresponsive, except for the w/c ratio of 0.60. Both cases are

369   related to the decrease of the wavelength, as can be seen in Table 1-3, also the asses of the degree

370   of carbonation had a strong correlation to the one obtained with the FTIR results.

371   In the case of the results show in Figure 4e and 5e, the carbonation index had the strongest

372   correlation with the FTIR data of all measurements. This behavior was due to the small

373   wavelength, as show in table 1-3, and the property of the longitudinal waves to travel true all

374   media, which allows the ultrasound wave, to interact with a larger amount of material without

375   losing energy, enabling a better assess of the carbonation degree, regardless of the w/c ratio.

376

377

378

5. Conclusions

379

The following conclusions are drawn based on the results obtained in this paper:

380

1. The non-destructive carbonation index based on ultrasound measurements, allows to determine the carbonation degree of the cement pastes studied (w/c = 0.60, 0.50 and 0.40), assuming that the carbonation products will progressively change the frequency spectra in time. The observed trends in the carbonation index are in agreement with the FTIR intensities observed for $CaCO_3$ generation.

2. For the cement pastes with w/c = 0.40, only the 250 kHz transversal wave transducer and the 500 kHz longitudinal wave transducer permit detection of the carbonation.

3. The carbonation index associated to w/c = 0.50 had a strong correlation with the FTIR results, especially with the 100 and 250 kHz longitudinal wave transducers.

4. The 250 kHz longitudinal wave transducers were able to distinguish between the carbonated and control specimens, as well as to assess the degree of carbonation in the w/c = 0.60, despite the atypical behavior of the control specimen.

References

[1]. L. Bertolini, B. Elsener, P. Pedeferri, E. Redaelli, R.B. Polder, Corrosion of Steel in Concrete: Prevention, Diagnosis, Repair, John Wiley & Sons, 2013

[2]. J.P. Broomfield, Corrosion of Steel in Concrete: Understanding, Investigation and Repair, CRC Press, 2002.

[3]. Neville, A. M., & Brooks, J. J. (1987). Concrete technology.

[4]. V. Papadakis, M. Fardis, C. Vayenas, Effect of composition, environmental factors and cement-lime mortar coating on concrete carbonation, Mater. Struct. 25 (5) (1992) 293–304.

[5]. N. Hyvert, A. Sellier, F. Duprat, P. Rougeau, P. Francisco, Dependency of C–S–H carbonation rate on CO_2 pressure to explain transition from accelerated tests to natural carbonation, Cem. Concr. Res. 40 (11) (2010) 1582–1589.

[6]. C.D. Atis, Accelerated carbonation and testing of concrete made with fly ash, Constr. Build. Mater. 17 (3) (2003) 147–152.

[7]. Papadakis, V. G., Vayenas, C. G., & Fardis, M. N. (1991). Physical and chemical characteristics affecting the durability of concrete. Materials Journal,88(2), 186-196.

[8]. P.H. Borges, J.O. Costa, N.B. Milestone, C.J. Lynsdale, R.E. Streatfield, Carbonation of CH and C–S–H in composite cement pastes containing high amounts of BFS, Cem. Concr. Res. 40 (2) (2010) 284–292.

[9]. S. Roy, K. Poh, D. Northwood, Durability of concrete—accelerated carbonation and weathering studies, Build. Environ. 34 (5) (1999) 597–606.

[10]. Chang, C. F., & Chen, J. W. (2006). The experimental investigation of concrete carbonation depth. Cement and Concrete Research, 36(9), 1760-1767.

426 [11]. T. Fukushima, Y. Yoshizaki, F. Tomosawa, K. Takahashi, Relationship between

427 neutralization depth and concentration distribution of CaCO3–Ca(OH)2 in

428 carbonated concrete, V.M. Malhotra (Ed.), Advances in Concrete Technology, ACI

429 SP–179, Tokushima, Japan (1998), pp. 347–363.

430 [12]. V.G. Papadakis, M.N. Fardis, C.G. Vayenas, Hydration and carbonation of

431 pozzolanic cements, ACI Mater. J., 89 (2) (1992), pp. 119–130.

432 [13]. X.F. Gao, Y. Lo, C.M. Tam, C.Y. Chung, Analysis of the infrared spectrum and

433 microstructure of hardened cement paste, Cem. Concr. Res., 29 (1999), pp. 805–812.

434 [14]. Villain, G., & Thiery, M. (2006). Gammadensimetry: A method to determine drying

435 and carbonation profiles in concrete. NDT & E International, 39(4), 328-337.

436 [15]. Chaix, J. F., Garnier, V., & Corneloup, G. (2003). Concrete damage evolution

437 analysis by backscattered ultrasonic waves. NDT & E International, 36(7), 461-469.

438 [16]. Vincent Garnier, Bogdan Piwakowski, Odile Abraham, Géraldine Villain, Cédric

439 Payan, Jean François Chaix, Acoustic techniques for concrete evaluation:

440 Improvements, comparisons and consistency Construction and Building Materials,

441 43 (2013), pp. 598–613.

442

443 [17]. Cosmes-López, M. F., Castellanos, F., & Cano-Barrita, P. F. D. J. (2017). Ultrasound

444 frequency analysis for identification of aggregates and cement paste in concrete.

445 Ultrasonics, 73, 88-95.

446

447 [18]. ASTM C31 / C31M-15ae1, Standard Practice for Making and Curing Concrete Test

448   Specimens in the Field, ASTM International, West Conshohocken, PA, 2015

449 [19]. Parrott, L. J., & Killoh, D. C. (1989). Carbonation in a 36 year old, in-situ concrete.

450   Cement and Concrete Research, 19(4), 649-656.

451

452 [20]. Mehta, P. K. (1986). Concrete. Structure, properties and materials.

453

454 [21]. P. Duhamel, M. Vetterli, Fast fourier transforms: A tutorial review and a state of the

455   art, Signal Processing 19 (1990), 259-299.

456

457 [22]. P. Anugonda, J. S. Wiehn, J. A. Turner, Diffusion of ultrasound in concrete,

458   Ultrasonics 39 (2001), 429–435.

459

460 [23]. A. Villarreal, S. Solis-Najera, L. Medina-Gómez, Application of Waterman-Truell

461   and the Dynamic Generalized Self-consistent Models on Concrete, Physics Procedia

462   70 (2015), 437 – 441.

463

464 [24]. Punurai, W., Jarzynski, J., Qu, J., Kurtis, K. E., & Jacobs, L. J. (2006).

465   Characterization of entrained air voids in cement paste with scattered ultrasound.

466   NDT & E International, 39(6), 514-524.

467

468 [25]. Punurai, W., Jarzynski, J., Qu, J., Kim, J. Y., Jacobs, L. J., & Kurtis, K. E. (2007).

469   Characterization of multi-scale porosity in cement paste by advanced ultrasonic

470   techniques. Cement and Concrete Research, 37(1), 38-46.

471 [26]. Qasrawi, H. Y. (2000). Concrete strength by combined nondestructive methods

472   simply and reliably predicted. Cement and concrete research, 30(5), 739-746.

473 [27]. F. Aydin, M. Saribiyik, Correlation between Schmidt Hammer and destructive

474   compressions testing for concretes in existing buildings, Sci. Res. Essays 5 (13)

475   (2010) 1644–1648.

476 [28]. Cagnon, H., Vidal, T., Sellier, A., Soula, C., Bourbon, X., & Camps, G. (2016).

477   Effects of water and temperature variations on deformation of limestone aggregates,

478   cement paste, mortar and High Performance Concrete (HPC). Cement and Concrete

479   Composites, 71, 131-143.

480

481 [29]. Chekroun, M., Le Marrec, L., Abraham, O., Durand, O., & Villain, G. (2009).

482   Analysis of coherent surface wave dispersion and attenuation for non-destructive

483   testing of concrete. Ultrasonics, 49(8), 743-751.

484

485 [30]. Métais, V., Chekroun, M., Le Marrec, L., Le Duff, A., Plantier, G., & Abraham, O.

486   (2016). Influence of multiple scattering in heterogeneous concrete on results of the

487   surface wave inverse problem. NDT & E International, 79, 53-62.

488

489 [31].   Chaix, J. F., Garnier, V., & Corneloup, G. (2006). Ultrasonic wave propagation in

490   heterogeneous solid media: Theoretical analysis and experimental

491   validation.Ultrasonics, 44(2), 200-210.

492

493 [32].   Akkaya, Y., Voigt, T., Subramaniam, K. V., & Shah, S. P. (2003). Nondestructive

494   measurement of concrete strength gain by an ultrasonic wave reflection method.

495   Materials and Structures, 36(8), 507-514.

496 [33].   Abo-Qudais, S. A. (2005). Effect of concrete mixing parameters on propagation of

497   ultrasonic waves. Construction and building materials, 19(4), 257-263.

498 [34].   Thiery, M., Villain, G., Dangla, P., & Platret, G. (2007). Investigation of the

499   carbonation front shape on cementitious materials: effects of the chemical kinetics.

500   Cement and Concrete Research, 37(7), 1047-1058.

Capítulo III

Ultrasound determination of chloride presence in cement paste

Mario F. Cosmes-López[1], Francisco Castellanos[2*], Prisciliano F. de J. Cano-Barrita[2], Arturo E. Ramírez-Ortiz[1]

[1] *PhD student at Instituto Politecnico Nacional, CIIDIR Unidad Oaxaca, Hornos No. 1003, Santa Cruz Xoxocotlán, Oaxaca, Mexico, C.P. 71230.*

[2] *Researcher at Instituto Politecnico Nacional, CIIDIR Unidad Oaxaca, Hornos No. 1003, Santa Cruz Xoxocotlán, Oaxaca, Mexico, C.P. 71230.*

Phone: + 52 951 5170610, Emails: mcosmesl1200@alumno.ipn.mx, fcastellanos@ipn.mx, pcano@ipn.mx and arturo_iciv@hotmail.com

*Corresponding author

Abstract

18   Durability of concrete structures depends on ability of the cover concrete to resist penetration of

19   harmful substances. Chloride ingress disrupts the passive film formed on the steel surface

20   causing corrosion. Traditional techniques used to determine chloride penetration involve

21   destructive sampling and chemical analysis. In order to improve some properties of concrete,

22   Portland cement is partially substituted with mineral additions such as silica fume and fly ash.

23   This study is focused on the ability of longitudinal and transversal ultrasound waves to detect the

24   presence of chlorides in cement paste specimens containing mineral admixtures. Eighteen

25   cylindrical specimens measuring 65 mm in diameter and 100 mm in height were cast with a w/c

26   ratio of 0.55, with 100% of ordinary Portland cement, 20% and 40% substitution of cement by

27   class F fly ash and 10% substitution by silica fume. The specimens were moist-cured in a

28   saturated lime solution at 23 ± 2 °C for 120 days to reach a high degree of hydration. After oven-

29   drying to constant mass, three samples of each group were vacuum saturated (4.08 bar) with

30   NaCl solutions of 0%, 16.5 % (2.8 M), and 33 % (5.6 M). Ultrasonic measurements were

31   undertaken at 0, 1, 3, 7 and 14 days using ultrasonic transducer with frequencies ranging from 50

32   kHz to 2250 kHz. Results show that it is possible to distinguish between the samples with and

33   without chlorides regardless of the mineral addition and between the mineral additions

34   depending on its binding capacity.

35   **Keywords:** Chloride binding, ultrasound, fly ash, silica fume

1. Introduction

Chloride penetration leads to corrosion of the reinforcing steel in concrete structures [1]. Chlorides may already be present in the materials employed for the elaboration of concrete but normally they ingress from external sources such as marine environments or deicing salts [2]. Cement hydration products react to some extent with chlorides to form Friedel's salt, leaving some free chloride ions that are responsible for the steel corrosion [3,4]. Therefore, the chloride binding capacity of cement paste is an important factor that influences the durability of concrete structures exposed to chloride-rich environments [5,6].

The use of mineral admixtures, such as fly ash and silica fume, increases the chloride binding capability of cement paste depending on the degree of substitution of Portland cement [7]. Chloride ion ingress into the cover concrete occurs mainly by diffusion due to a concentration gradient. The rate of diffusion is controlled by the chemical and physical characteristics of the pore structure [8]. Chloride ingress also depends on the surface concentration, as well as environmental factors such as temperature and relative humidity [9], producing a non-uniform distribution of chloride ions in concrete [10]. In the case of partially saturated cover concrete, water will be drawn into the pore structure driven by capillary forces [11].

Determination of chloride ion content in concrete is performed by different methods such as Accelerated Chloride Penetration [12], which is used to determine the apparent coefficient of chloride ion diffusion into concrete. A reliable chloride concentration profile for high quality concrete is difficult to obtain, as the penetration depth may be insufficient at 90 days [13].

56   The Electrical Indication of Concrete Ability to Resist Chloride Ion Penetration [14] is a rapid

57   test to determine concrete relative resistance to penetration chloride ions. The electrical

58   resistivity assesses chloride ingress considering that chloride presence increases the electrical

59   conductivity of concrete. Since electrical current is used, it affects all ions in the pore solution,

60   not just chloride ions. Also, the measurements are made before a steady migration is achieved

61   and the high voltage increases the temperature that affects the results.

62   Another method is the Electrical Migration Technique [15] which accelerates the movement of

63   chloride ions by the use of a low intensity electrical field. Despite of reducing the temperature

64   related to the use of an electrical current, there is still a significant drawback due to the

65   employment of an electrical migration test.

66   The Ion Selective Electrode Method [16] determines free chlorides with an embedded sensor that

67   assesses changes in potential related to chemical activity. Unfortunately, the range of evaluation

68   is too narrow to assure a reliable measurement. These non-destructive methods are very sensitive

69   to the moisture content and require a calibration relationship to ensure repeatability [17].

70   Ultrasound techniques such as ultrasound pulse velocity have been employed to detect the

71   presence of internal defects in concrete structures. Low ultrasound frequency (50 kHz) are used

72   for characterization of large defects [18]. Higher frequencies (0.5-1 MHz) have been

73   demonstrated to be more suitable for detection of smaller variations related to concrete

74   degradation [19]. The ultrasound pulse velocity is capable of detecting microstructural changes.

75   The presence of cracks or aggregates in concrete strongly influence the scattering when the

76   wavelength is of the same order, diminishing the sensitivity to such defects/components [20].

77 In this study, a signal processing technique of longitudinal and transversal waves produced at

78 different frequencies was used for detecting the presence of chlorides in cement pastes with and

79 without mineral additions. In order to increase the surface exposed to chloride binding,

80 specimens were oven-dried to evaporate the free water and replace it with NaCl solutions at

81 different concentrations.

82 2. Experimental procedure

83 2.1. Materials

84 Mexican ordinary Portland cement class 30RS (ASTM C150 Type I) was used. Eighteen

85 cylindrical specimens measuring 65 mm in diameter and 100 mm in height were cast with a w/c

86 ratio of 0.55, with 100% of ordinary Portland cement (OPC), 20% and 40% substitution of

87 cement by class F fly ash (20FA and 40FA, respectively) and 10% substitution by silica fume

88 (10SF). The cylinders were filled in two layers, compacted by applying sixty strokes on the base

89 of the mold on each layer. Then the specimens were placed in a device designed to rotate the

90 samples at a speed of 7 rpm to avoid sedimentation. After 1 day, the specimens were stripped and

91 moist-cured in a saturated lime solution at 23 ± 2 °C for 120 days to ensure complete hydration,

92 according to the standard ASTM C31 [21].

93 In order to have similar initial conditions, all specimens were vacuum saturated with deionized

94 water for at least one hour to ensure full saturation. Then the specimens were weighed and placed

95 in an oven at 105 °C for two days, until constant mass is achieved. Once the specimens reached

96 room temperature, three specimens of each group were vacuum saturated (4.08 bar) with NaCl

97   solutions of 16.5 % (2.8 M), 33 % (5.6 M) and one with only deionized water. All samples were

98   covered with parafilm to prevent moisture loss.

99   **2.2. Method**

100   **2.2.1. Ultrasonic measurements**

101   To perform ultrasonic measurements, transducers were placed and centered on the circular faces.

102   The pressure exerted on the transducers was controlled by a constant mass of 2.5 kg. The same

103   position of the transducers was kept in through transmission measurements at different times.

104   Ultrasonic measurements were made at 0, 1, 3, 7 and 14 days with transducer frequencies

105   ranging from 50 kHz to 2250 kHz, for the three solutions used (NaCl 0% (deionized water),

106   16.5% NaCl and 33% NaCl).

107   **2.2.2. Determination of chloride binding isotherms by the equilibrium method**

108   This method assumes that once the equilibrium between the external solution and the pore

109   solution of the sample is reached, the reduction in the concentration of the external solution is

110   due to chlorides bound by cement hydration products. Therefore, by knowing the initial and final

111   concentrations, the volume of the external solution and the dry mass of the sample, it is possible

112   the calculation of the amount of bound chlorides according to [22]:

113    $$C_b = \frac{35.453\ (C_i - C_e)}{w_{11}(1 - \xi_{11})} \tag{1}$$

114   where C_b is the amount of bound chlorides in mg $Cl/$ per sample, V is the volume of the

115   external solution in mL, C_i is the external solution initial concentration of chlorides in mol / L, C_e

116   is the concentration of free chlorides in equilibrium with the external solution in mol / L, 35,453

117   is the molar mass of chloride ion, w_{11} is the mass in grams of the sample at a relative humidity

118   (RH) of 11% and ξ_{11} is the evaporable water content to 11% RH. The chloride isotherms for

119   each cementitious system are shown in Fig. 1.
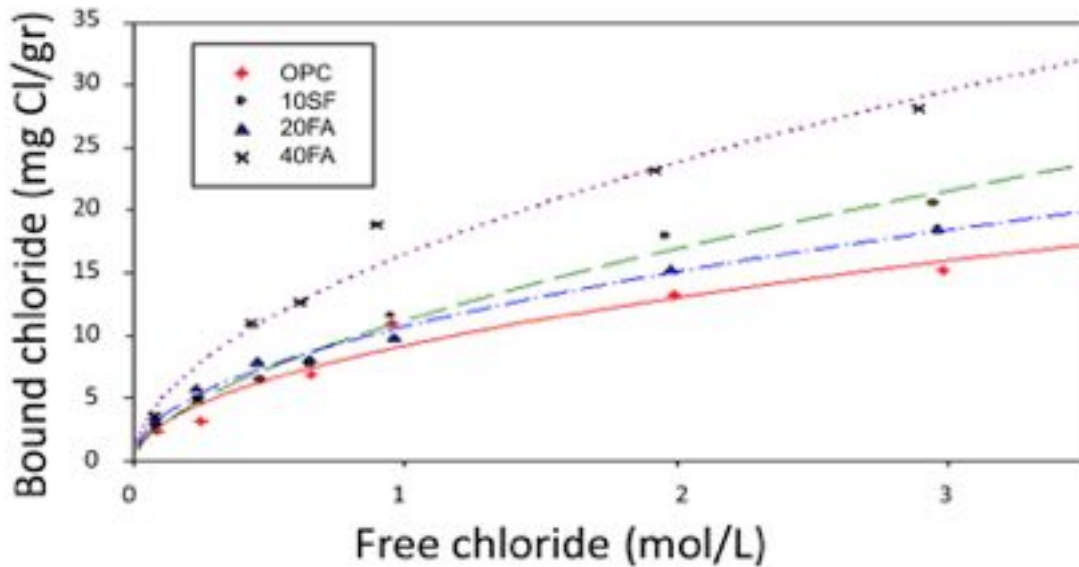
120

121   Fig. 1. Chloride binding isotherms for the four cementitious systems at a temperature of 23 °C

122   for different chloride concentrations [23].

3. Wave analysis

123

3.1. Ultrasound signal processing

124

125   The herein proposed ultrasound signal processing to assess the presence of chlorides in the

126   specimens was based on the method proposed in our previous work [24], to obtain a bound

127   chloride index.

128   Ic=I-A   (2)

129   However, in order to distinguish between NaCl concentrations inside the different cement pastes,

130   a standard deviation of the response of each concentration was obtained with respect to the

131   response of water-saturated specimens.

4. Results and discussion

133   Fig. 2 shows the bound chloride index for the distinct cement pastes using the 50 kHz transverse

134   wave transducers. Oven drying the samples caused extensive cracking that influenced the

135   ultrasonic response of the cement pastes. This influence can be seen on the samples containing

136   water. These specimens present changes that cannot be attributed to the hydration process as the

137   samples were moist cured for an adequate period of time to ensure a high degree of hydration.

138
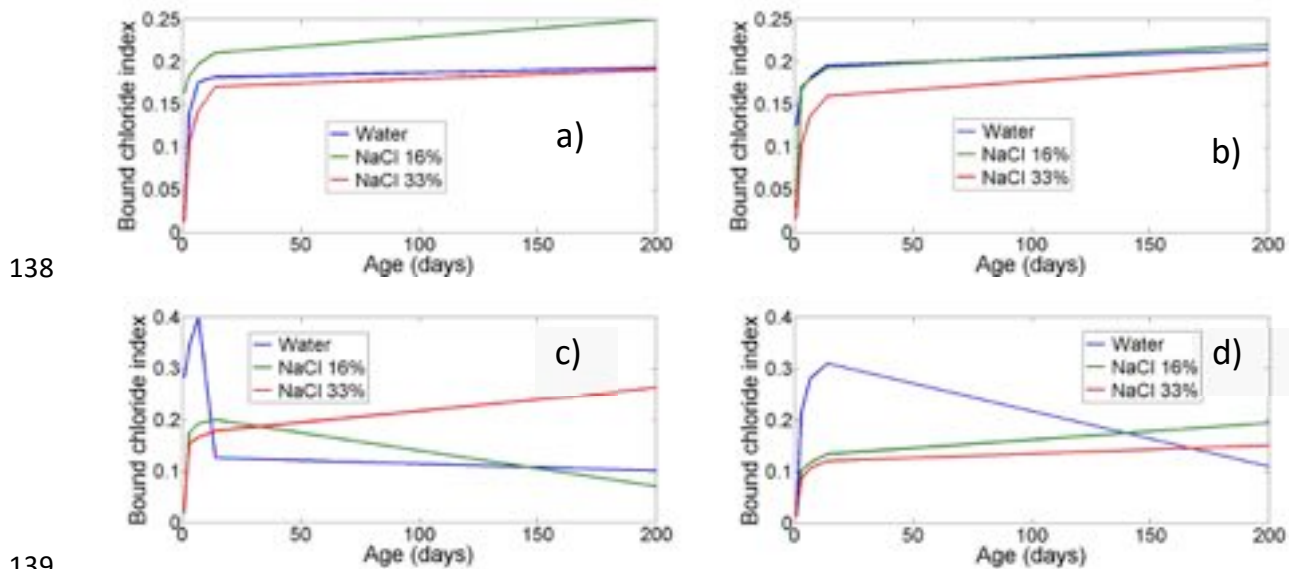
139

140   Fig. 2. Bound chloride Index obtained for all cement paste specimens containing a) 100 %

141   Portland cement, b) 10% silica fume, c) 20 % fly ash, and d) 40 % fly ash. Transversal wave

142   transducers of 50 kHz were employed.

143   These changes may be attributed to the movement of water inside the cement paste after vacuum

144   saturation. It is possible that water did not completely filled all the gel pores. As a result,

145   moisture redistribution by capillary forces may occur [25]. In addition, it is not expected that the

146   penetration of water would significantly change the microstructure of the samples. On the other

147   hand, chloride chemical binding will produce crystals of Friedel's salt that may affect the

148   ultrasound response of the samples. It is possible to assess these changes by comparing the index

149   obtained from the different chloride concentration specimens with the control specimen that

150   contains only water.

151   The increase in concentration of the NaCl solutions inside the specimens will in turn increase the

152   viscosity of the pore solution. Higher NaCl concentrations will also increase the amount of

153   chemically and physically bound chlorides in the cement pastes [26, 27, 28, 29], provided the

154   binding capacity is not exhausted. This will emphasize the different behavior among the

155   specimens saturated with different concentrations (0%, 16% and 33% of NaCl). Changes in the

156   microstructure of the different pastes are due to higher concentration of free chlorides in the pore

157   solution that reacts with C3A [27]. The latter changes depicted, are reflected in the higher

158   deviation from the specimens containing water.

159   As can be seen in Fig. 3, it is possible to distinguish the behavior between specimens containing

160   NaCl solutions with different concentrations, aside of the transducer employed, due to the

161   difference in average values of standard deviations.

162
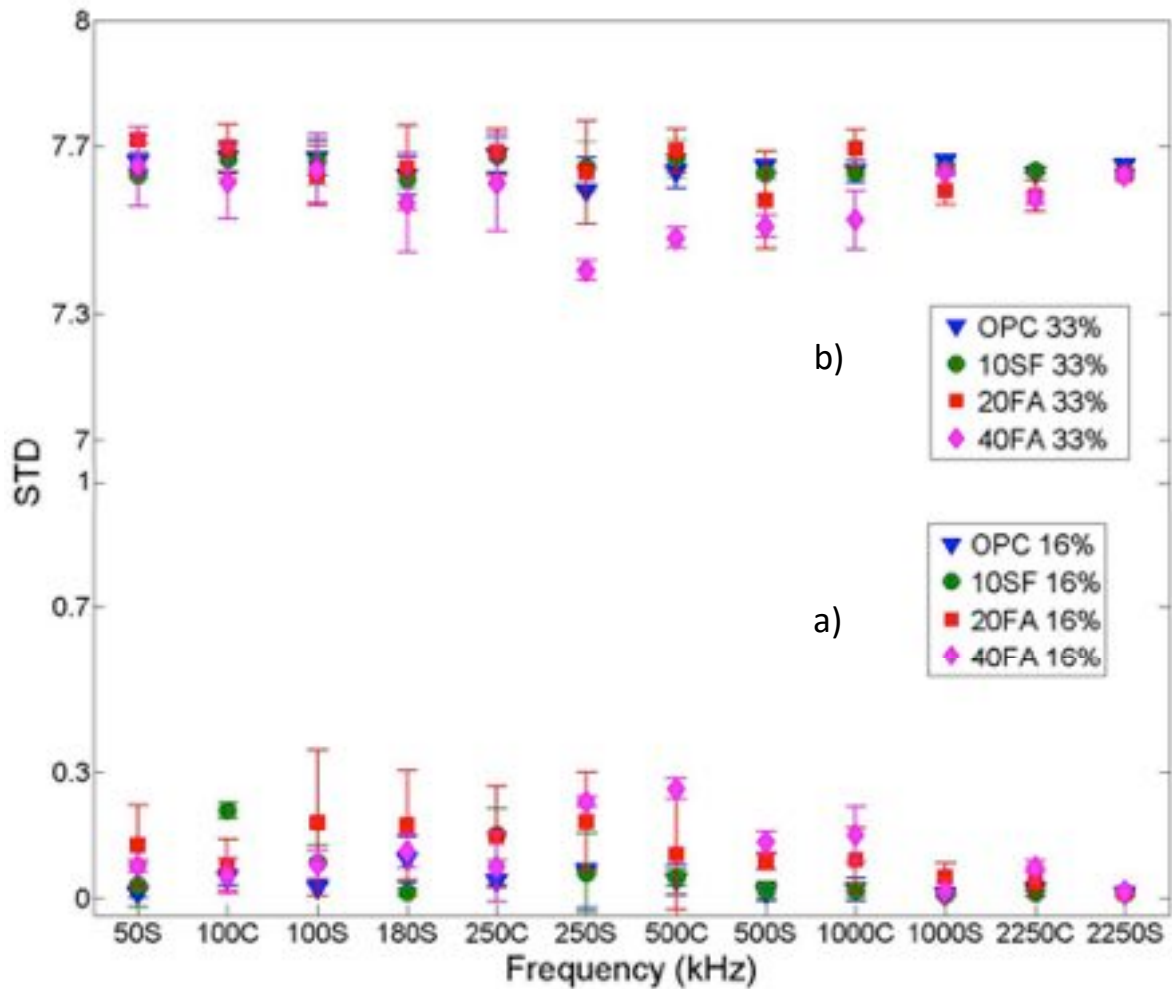
Fig. 3. Average values of the standard deviation obtained from a) 16 % NaCl solution, and b) 33
% NaCl solution, assuming as a mean of the process the response of the control specimens
containing water, for all ultrasound transducers used.

Fig. 4 presents the standard deviation of the cement paste specimens with a 16% concentration of
NaCl versus the control specimens containing water, for all ultrasound transducers. It is observed
that the standard deviation is very low compared with the 33% concentration specimens.
However, as shown in Fig. 4a, the low frequency transducers (50 to 180 kHz) are not sensitive to
the microstructural changes, unlike the frequencies of 250 and 500 kHz, that are consistent with

171   the chloride binding isotherms shown in Fig. 1. This behavior may be associated with the higher

172   sensitivity related to the higher frequencies employed, as well as by the preference of transversal

173   waves to travel through the solid phase of the porous medium, modified by the formation of

174   Friedel's salt [30].

175   In the case of Fig. 4b, transducers with frequencies from 500 to 2250 kHz show a similar

176   behavior compared with the results of the chloride binding isotherms (Fig. 1). This behavior is

177   not only due to wavelength but also because of the capability of the longitudinal waves to travel

178   through fluid and solid media. Despite of this distinction, the reduction of the concentration of

179   NaCl in the pore solution and the binding of the cement paste through the formation of Friedel's

180   salt is more difficult to differentiate with this type of waves.

181   As can be seen, the longitudinal wave transducer from 500 kHz and above, had a better

182   distinction between the four types of cement paste than the transversal wave transducer. At lower

183   frequencies, the results are not consistent.
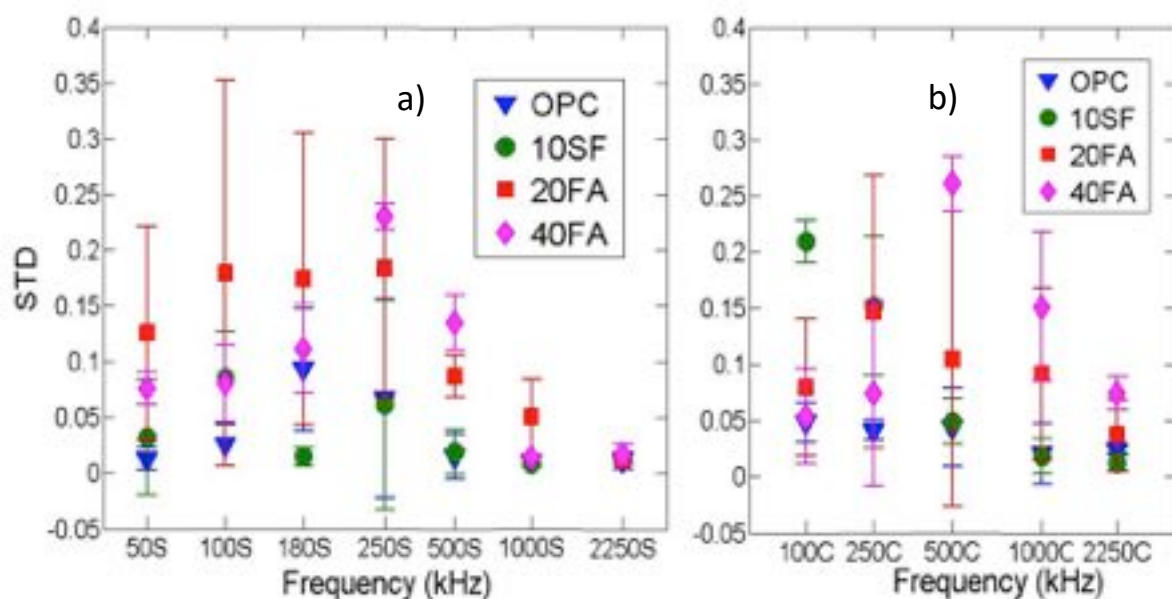
184

185   Fig. 4. Average values of standard deviation for 16 % NaCl solution of all cement paste samples

186   using a) transversal wave transducers, and b) longitudinal wave transducers.

187   Fig. 5 shows results for the measurements on samples saturated with 33 % NaCl solution

188   concentration. As can be seen, the standard deviation is higher than that of the 16 % NaCl

189   concentration. In Fig. 5a the results of the transversal wave transducers show a lower dispersion

190   of data, in comparison with the last concentration (Fig. 4a). The main feature is that the cement

191   paste which has the highest binding capacity (40FA) produces a lower average value of the

192   standard deviation than the other samples. These results may be attributed to the high chloride

193   concentration, that caused an increase in the pore solution viscosity [31], decreasing the

194   propagation through the pore structure. Another possible factor is the chemical chloride binding

195   that obstructs the movement of the pore solution, and subsequently decreasing the ultrasound

196   signal changes [32]. That may be the main reason why the most reactive cement paste is lower

197   than the other cement pastes in all transducer frequencies (Fig. 5). However, the preference of

198   the transversal wave to travel only through the solid phase impact on the high dispersion of the

199   results. The results of the 250 kHz transversal wave transducer show an acceptable

200   differentiation among the different cement pastes

201   Results of the longitudinal wave transducers are shown in Fig. 5b. As can be seen, the behavior

202   is very similar to the transversal wave transducer. However, since the longitudinal waves are able

203   to travel through fluid and solid media, the resulting data dispersion is lower than that of the

204   transversal wave transducers. The higher frequencies ranging from 500 and 1000 kHz present a

205   better differentiation among cement pastes. Unlike the results for 16% NaCl, in this case even for

206   the lower frequencies it is possible to distinguish the different cement pastes

207
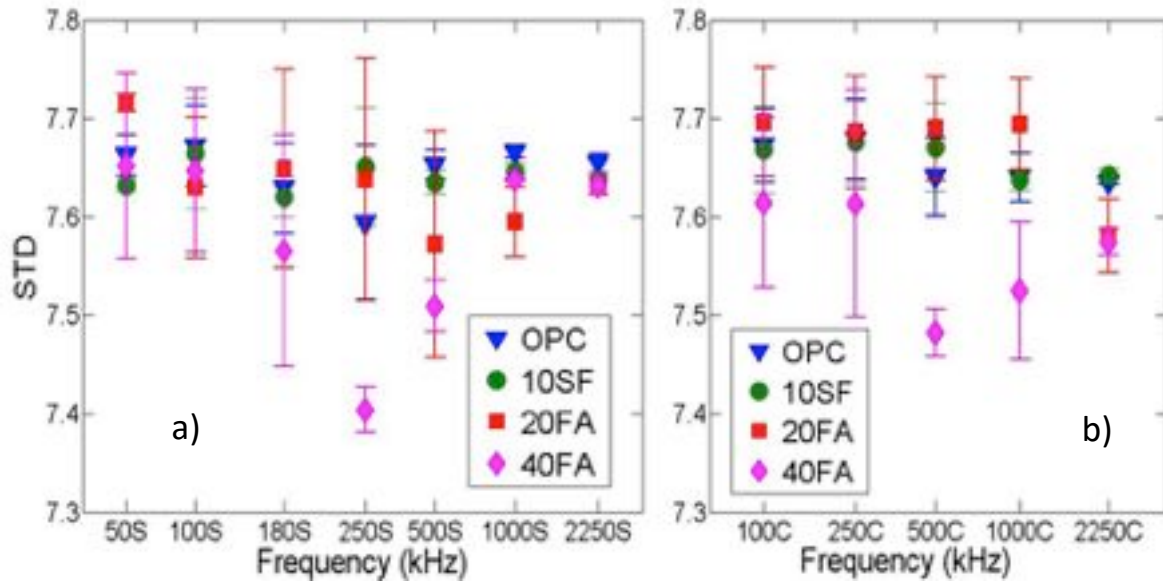
Fig. 5. Average values of standard deviation for 33% NaCl solutions for all cement paste

209 specimens, a) transversal wave transducer, and b) longitudinal wave transducer.

210

211

212

213

214

215

216

217

218

219

220

5. Conclusions

221

222 1. It is possible to distinguish between the chloride concentrations of the solutions

223   employed for saturating the samples (0 %, 16 % and 33 %) considering as reference

224   the deionized water saturated specimens. This applies for all four-different cement

225   pastes.

226 2. The results obtained with the proposed methodology, for the 16 % NaCl concentration

227   it is consistent with the chloride binding isotherms, better identified with the 250 and

228   500 kHz transversal wave transducer and longitudinal wave transducer with

229   frequencies of 500 kHz and higher, despite the extensive cracking of the specimens

230   due to oven drying.

231 3. Results of the ultrasound signals analysis obtained with the methodology proposed, for

232   the specimens saturated with 33 % NaCl concentration, are explained by the high

233   concentration of chloride in the pore solution that increase the amount of chloride

234   bound in the cement pastes, consuming the aluminates. This can be better appreciated

235   in 250 kHz transversal wave transducer and for 500 and 1000 kHz longitudinal wave

236   transducer.

237

References

238   **References**

239   [1]. Sánchez, I., Nóvoa, X. R., De Vera, G., & Climent, M. A. (2008). Microstructural
240   modifications in Portland cement concrete due to forced ionic migration tests. Study
241   by impedance spectroscopy. Cement and Concrete Research, 38(7), 1015-1025.

242   [2]. Neville Adam, Chloride attack of reinforced concrete: an overview, Materials and
243   Structures (1995), Vol. 28, pp.63-70

244   [3]. G.K. Glass, N.M. Hassanein, N.R. Buenfeld, Magazine of Concrete Research 49
245   (1997) 323.

246   [4]. K. Byfors, Chloride initiated reinforcement corrosion, CBI Report 1:90, Swedish
247   Cement and Concrete Research Institute, Stockholm, 1990, p. 5.

248   [5]. T. Luping, L.-O. Nillsson, Chloride binding capacity and binding isotherms of OPC
249   pastes and mortars, Cem. Concr. Res. 23 (2) (1993) 247– 253.

250   [6]. P.S. Mangat, B.T. Molloy, Chloride binding in concrete containing PFA, gbs or silica
251   fume under sea water exposure, Mag. Concr. Res. 47 (171) (1995) 129– 14

252   [7]. Mangat, P. S., & Molloy, B. T. (1995). Chloride binding in concrete containing PFA,
253   GBS or silica fume under sea-water exposure. Magazine of concrete research,
254   47(171), 129-141.

255   [8]. Detwiler, R. J., Kjellsen, K. O., & Gjorv, O. E. (1991). Resistance to chloride
256   intrusion of concrete cured at different temperatures. Materials Journal, 88(1), 19-24.

257   [9]. Bastidas-Arteaga, E., Chateauneuf, A., Sánchez-Silva, M., Bressolette, P., &
258   Schoefs, F. (2010). Influence of weather and global warming in chloride ingress into
259   concrete: A stochastic approach. Structural Safety, 32(4), 238-249.

260 [10]. Halamickova, P., Detwiler, R. J., Bentz, D. P., & Garboczi, E. J. (1995). Water

261   permeability and chloride ion diffusion in Portland cement mortars: relationship to

262   sand content and critical pore diameter. Cement and Concrete Research, 25(4), 790-

263   802.

264 [11]. Delagrave, A., Marchand, J., & Samson, E. (1996). Prediction of diffusion

265   coefficients in cement-based materials on the basis of migration experiments.

266   Cement and Concrete Research, 26(12), 1831-1842.

267 [12]. Nordtest Method NT BUILD 443: Accelerated Chloride Penetration into Hardened

268   Concrete, Nordtest, Espoo, Finland, Proj. 1154-94, 1995.

269 [13]. "Standard Method of Test for Resistance of Concrete to Chloride Ion Penetration",

270   (T259-80), American Association of State Highway and Transportation Officials,

271   Washington, D.C., U.S.A., 1980

272 [14]. Andrade, C. "Calculation of Chloride Diffusion Coefficients in Concrete From Ionic

273   Migration Measurements" Cement and Concrete Research, Vol. 23, No, 3, pp. 724-

274   742, 1993

275 [15]. Andrade, C. "Calculation of Chloride Diffusion Coefficients in Concrete From Ionic

276   Migration Measurements" Cement and Concrete Research, Vol. 23, No, 3, pp. 724-

277   742, 1993

278 [16]. Muralidharan, S., Vedalakshmi, R., Saraswathi, V., Joseph, J., & Palaniswamy, N.

279   (2005). Studies on the aspects of chloride ion determination in different types of

280   concrete under macro-cell corrosion conditions. Building and environment, 40(9),

281   1275-1281.

282

283 [17]. Basheer, P. A. M., Gilleece, P. R. V., Long, A. E., & Mc Carter, W. J. (2002).

284 Monitoring electrical resistance of concretes containing alternative cementitious

285 materials to assess their resistance to chloride penetration. Cement and Concrete

286 Composites, 24(5), 437-449.

287 [18]. Basheer, P. A. M., Gilleece, P. R. V., Long, A. E., & Mc Carter, W. J. (2002).

288 Monitoring electrical resistance of concretes containing alternative cementitious

289 materials to assess their resistance to chloride penetration. Cement and Concrete

290 Composites, 24(5), 437-449.

291 [19]. Naffa, S. O., Goueygou, M., Piwakowski, B., & Buyle-Bodin, F. (2002). Detection

292 of chemical damage in concrete using ultrasound. Ultrasonics, 40(1), 247-251.

293

294 [20]. ChaixJF, GarnierV, CorneloupG. Ultrasonic wave propagation in hetero-geneous

295 solid media: theoretical analysis and experimental validation. Ultrasonics 2006;

296 44:200–10.

297

298 [21]. ASTM C31 / C31M-15ae1, Standard Practice for Making and Curing Concrete Test

299 Specimens in the Field, ASTM International, West Conshohocken, PA, 2015.

300

301 [22]. Luping, T., & Nilsson, L. O. (1993). Chloride binding capacity and binding

302 isotherms of OPC pastes and mortars. Cement and concrete research, 23(2), 247-253.

303

304 [23]. Arturo Emanuel Ramírez Ortiz, Ultrasonido aplicado al estudio de la penetración y

305   ligado de cloruros en pastas de cemento, Master thesis, Instituto Politécnico

306   Nacional, 2012.

307

308 [24]. Cosmes-López, M. F., Castellanos, F., & Cano-Barrita, P. F. D. J. (2017). Ultrasound

309   frequency analysis for identification of aggregates and cement paste in concrete.

310   Ultrasonics, 73, 88-95.

311 [25]. Kanematsu, M., Maruyama, I., Noguchi, T., Iikura, H., & Tsuchiya, N. (2009).

312   Quantification of water penetration into concrete through cracks by neutron

313   radiography. Nuclear Instruments and Methods in Physics Research Section A:

314   Accelerators, Spectrometers, Detectors and Associated Equipment, 605(1), 154-158.

315 [26]. Byfors, K., "Chloride Binding in Cement Paste", Nordic Concrete Research, Vol. 5,

316   pp. 27-38, 1986

317

318 [27]. Rasheeduzzafar, Dakhil, F.D., Bader, M.A. and Khan, M.M., "Performance of

319   Corrosion Resisting Steels in Chloride Bearing Concrete', ACI Materials Journal,

320   Vol. 89, No. 5, pp. 439-448, 1992.

321

322 [28]. Kestin, J., Khalifa, H. E., Ro, S. T., & Wakeham, W. A. (1977). Preliminary data on

323   the pressure effect on the viscosity of sodium chloride-water solutions in the range

324   10-40. degree. C. Journal of Chemical and Engineering Data, 22(2), 207-214.

325

326 [29].   Jacquemin, J., Husson, P., Padua, A. A., & Majer, V. (2006). Density and viscosity

327   of several pure and water-saturated ionic liquids. Green Chemistry, 8(2), 172-180.

328

329 [30].   Suryavanshi, A. K., Scantlebury, J. D., & Lyon, S. B. (1996). Mechanism of Friedel's

330   salt formation in cements rich in tri-calcium aluminate. Cement and concrete

331   research, 26(5), 717-727.

332 [31].   Chenlo, F., Moreira, R., Pereira, G., & Ampudia, A. (2002). Viscosities of aqueous

333   solutions of sucrose and sodium chloride of interest in osmotic dehydration

334   processes. Journal of food Engineering, 54(4), 347-352.

335 [32].   Sawamura, S., Yoshimura, Y., Kitamura, K., & Taniguchi, Y. (1992). Effects of

336   pressure, temperature, and concentration on the viscosity of an aqueous solution of

337   sodium chloride. The Journal of Physical Chemistry, 96(13), 5526-5529.